

Electronic Thesis and Dissertation Repository

4-30-2018 1:00 PM

Performance Enhancement by Exploiting the Spatial Domain for Cost, Space and Spectrum Constraint 5G Communication

Golara Zafari, *The University of Western Ontario*

Supervisor: Wang, Xianbin, *The University of Western Ontario*

A thesis submitted in partial fulfillment of the requirements for the Master of Science degree in Electrical and Computer Engineering

© Golara Zafari 2018

Follow this and additional works at: <https://ir.lib.uwo.ca/etd>



Part of the [Systems and Communications Commons](#)

Recommended Citation

Zafari, Golara, "Performance Enhancement by Exploiting the Spatial Domain for Cost, Space and Spectrum Constraint 5G Communication" (2018). *Electronic Thesis and Dissertation Repository*. 5400. <https://ir.lib.uwo.ca/etd/5400>

This Dissertation/Thesis is brought to you for free and open access by Scholarship@Western. It has been accepted for inclusion in Electronic Thesis and Dissertation Repository by an authorized administrator of Scholarship@Western. For more information, please contact wlsadmin@uwo.ca.

Abstract

With everlasting increase of connectivity demand and high speed data communication, lots of progresses have been made to provide a sufficient quality of services (QoS). Several advanced technologies have been the cornerstone of this trend in academia as well as in industry. Nevertheless, there are some implementation challenges, which needs to be closely investigated. In this thesis, among all challenges, we elaborate on those related to number of radio frequency (RF) chains and resource scarcity.

The principle idea behind our proposed initial solution is to exploit the spatial domain as an additional degree of freedom. To be more specific, we benefit from spatial domain and antenna index in a multiple-input multiple-output (MIMO) system with dual-polarized (DP) antennas to convey the information. We develop a two-stage algorithm to groups the antennas which ends up to the optimum performance. Another advantage of this proposed algorithm is the complete complexity reduction of exhaustive search over the whole available space.

Moreover, due to the continuous growth of demands which results in spectrum scarcity, we investigate the extension of long term evolution (LTE) spectrum. Such a paradigm shift is realized to offload part of the data to unlicensed band, which has been initially dedicated to other standardizations such as wireless local area networks (WLAN). As both LTE and wireless fidelity (Wi-Fi) networks have been widely deployed with solid infrastructures, it is significantly important to make their coexistence viable with a cost-effective approach which inherently requires the minimum protocol modification. Thus, we take the advantage of spatially located multiple antennas of base station (BS) and access point (AP) for the sake of beamforming and interference reduction.

In addition to network coexistence, we approach the resource scarcity from the non-orthogonal multiple access (NOMA) point of view, where users share the frequency and time resources and are differentiated in power domain. In particular, we closely consider those users with limited number of RF chains. Similar to our first approach, we utilize spatial modulation (SM) in user end and after evaluating their performance, we propose to consider the capacity of SM NOMA to elaborate the impact of pairing on the achievable sum rate performance.

Keywords: MIMO, SM, NOMA, antenna selection

Co-Authorship Statement

This thesis has been written by Golara Zafari under supervision of Dr. Xianbin Wang. The material presented in Chapter three and four have been published in IEEE Vehicular Technology Conference as follows

G. Zafari, M. Koca, X. Wang and M. G. S. Sriyananda, “Antenna Grouping in Dual-Polarized Generalized Spatial Modulation,” 2017 IEEE 86th Vehicular Technology Conference (VTC-Fall), Toronto, ON, 2017, pp. 1-6.

G. Zafari and X. Wang, “Cognitive Co-Existence of Unlicensed Wireless Networks through Beamforming,” 2017 IEEE 86th Vehicular Technology Conference (VTC-Fall), Toronto, ON, 2017, pp. 1-5.

Acknowledgements

First, I would like to express my sincere appreciation to my supervisor Dr. Xianbin Wang for his guidance and support. I would like to express my gratitude to Dr. Wang for providing me with the opportunity to work under his supervision. It was under his guidance and support that I was able to accomplish the program. I would also like to thank the examining committee, Dr. Shami, Dr. Badrkhani Ajaei, and Dr. Mao for their constructive suggestions on my research and thesis.

Special thanks to Dr. Junghoon Suh, Dr. Edward Au, and Dr. Osama AboulMagd from Huawei Corporation for their insightful hints and helpful discussions. My sincere appreciation to Dr. Koca for all his encouragements and valuable suggestions.

Words cannot express how grateful I am to have my lovely family. I would like to thank my parents for their endless love, support, and advice that always enlighten my way. Many thanks to my dear brother Zafar and his wife Elahe for making me so determined to achieve all my goals. I miss you all. I also feel so much fortunate to have my beloved husband, Behzad. His stubborn integrity, his knowledge, and his stickler of perfection were a true inspiration for me to accomplish this program.

Last but not least, I would like to thank all dear friends in our research team. Specially, Hessam, Sabin, Hao, Monica, Yanan, and Shery for all time we spend together

Contents

Abstract	ii
Co-Authorship Statement	iii
Acknowledgements	iv
List of Figures	viii
List of Tables	x
List of Abbreviations, Symbols, and Nomenclature	xi
1 Introduction	1
1.1 Overview of Promising Communication Technologies	1
1.2 Thesis Motivation	2
1.3 Thesis Objectives	3
1.4 Technical Contributions of the Thesis	4
1.5 Scope of Thesis	4
2 Principle and Detection Analysis of Spatial Modulation	6
2.1 Modulation in Space Domain	6
2.1.1 Spatial Modulation Technique	7
2.1.2 Multi-stream Generalized Spatial Modulation	10
2.2 Detection Algorithms	12
2.2.1 Low-complex Suboptimal Linear Detection	12
Zero Forcing (ZF) Detection Algorithm	12
Minimum Mean Square Error (MMSE) Detection Algorithm	13

2.2.2	Successive Interference Cancellation Detection	13
2.2.3	Optimal Maximum Likelihood Detection	13
2.2.4	Log-Likelihood Detection Algorithm	15
2.2.5	Performance Analysis of SM with Different Detection Algorithms	19
3	Antenna Selection in Dual-Polarized Generalized Spatial Modulation	23
3.1	Introduction	23
3.2	System Model	25
3.2.1	TITO Scenario	26
3.2.2	MIMO Scenario	27
3.3	Proposed Antenna Grouping	29
3.3.1	Selection of Group Indicators	29
3.3.2	Selection of Inner Group Antennas	30
3.3.3	Feasibility of the Algorithm	30
3.4	Performance Analysis	32
3.5	Simulation Results	33
3.6	Conclusion	35
4	Co-existence of LTE and Wi-Fi in Unlicensed Band	38
4.1	Introduction	38
4.2	System Model	40
4.3	Wi-Fi Received Power Minimization	42
4.4	UE Received SNR Maximization	44
4.5	Simulation Results	45
4.6	Conclusion	49
4.7	Proof of Proposition 4.3.1	50
5	NOMA-based Communication with Spatial Modulation	52
5.1	Introduction	52
5.2	System Model	54
5.3	Average Bit Error Rate Analysis	55

5.3.1	Simulation Results	57
5.4	User Pairing with Fixed Power Allocation	59
5.4.1	User pairing in SISO NOMA	60
5.4.2	User pairing in MIMO Scenario	69
5.5	Capacity of SM-NOMA	70
5.5.1	Simulation Results	74
6	Conclusion and Future Work	76
	Bibliography	77
	Curriculum Vitae	84

List of Figures

2.1	Illustration of SM transmission algorithm [1].	8
2.2	Successive interference cancellation approach [2].	14
2.3	Block diagram of SM transmission and ML detection structure [3].	15
2.4	Convolutional encoder with coding rate of 1/2 [4].	18
2.5	Performance analysis based on LLR detection.	18
2.6	Comparison of spatial multiplexing and spatial modulation, 6 bits/subcarrier. . .	20
2.7	Comparison of spatial multiplexing and spatial modulation, 10 bits/subcarrier. .	20
2.8	Comparison of MRC and ML detection of SM.	21
2.9	2×2 SM-MIMO and SMX comparison based on LLR detection, $R = 4$	22
2.10	4×4 SM-MIMO and SMX comparison based on LLR detection, $R = 4$	22
3.1	DP antenna configuration with different number of antennas, a) $N_t = 8$ DP antennas, b) $N_t = 4$ DP antennas.	29
3.2	An example of antenna grouping considering their distance and polarizations, assuming $N_t = 32$ DP antennas, $m = 3$, and $N_a = 2$	31
3.3	Performance comparison of the proposed algorithm with the optimum achievable ABEP and UP-GSM with different spatial correlation coefficients when $N_a = 2$, for a) $R = 3$ bpcu, b) $R = 4$ bpcu.	36
3.4	Performance comparison of the proposed algorithm with the optimum achievable ABEP and UP-GSM with different spatial correlation coefficients when $N_a = 3$, for a) $R = 3$ bpcu, b) $R = 4$ bpcu.	37
4.1	Networks coexistence and undesired interference from LTE-U on Wi-Fi.	41
4.2	Minimum received power by Wi-Fi AP vs. QoS threshold for UE, $\alpha_g = -10$ dB and $\alpha_h = \{-20, -10, 0\}$	47

4.3	Minimum received power by Wi-Fi AP vs. QoS threshold for UE, $\alpha_h = -10$ dB and $\alpha_g = \{-20, -10, 0\}$	48
4.4	Maximum received SNR by UE vs. power threshold for Wi-Fi AP, $\alpha_g = -10$ dB and $\alpha_h = \{-20, -10, 0\}$	49
4.5	Maximum received SNR by UE vs. power threshold for Wi-Fi AP, $\alpha_h = -10$ dB and $\alpha_g = \{-20, -10, 0\}$	50
5.1	Principal of NOMA communication with SIC detection [5].	53
5.2	Performance analysis of two users with NOMA transmission and same spectral efficiencies, i.e., $R = 4$	58
5.3	Performance analysis of two users with NOMA transmission and different spectral efficiencies and different number of antennas.	59
5.4	Capacity comparison of NOMA and OMA, SISO, $\alpha_n^2 = 1/5$ and $\alpha_m^2 = 4/5$, $K = 0$. 61	
5.5	Capacity comparison of NOMA and OMA, SISO, $\alpha_n^2 = 1/5$ and $\alpha_m^2 = 4/5$, $K = 5$. 61	
5.6	Capacity comparison of NOMA and OMA, SISO, $\alpha_n^2 = 1/5$ and $\alpha_m^2 = 4/5$, $SNR = 20$ dB.	62
5.7	Probability of OMA outperforming NOMA vs. $1/N_0$, $K = 0$	68
5.8	Probability of OMA outperforming NOMA vs. $1/N_0$, $K = 5$	68
5.9	User pairing based on sum rate capacity, $\alpha_1^2 = 1/5$ and $\alpha_2^2 = 4/5$, $N_t = N_r = 4$	74
5.10	Capacity comparison between SM-NOMA and SM-OMA, $\alpha_1^2 = 1/5$ and $\alpha_2^2 = 4/5$, $N_t = N_r = 4$	75

List of Tables

2.1	SM scheme, Mapping input bits to corresponding constellation symbols and antenna space.	9
2.2	G-SM scheme, Mapping input bits to corresponding constellation symbols and antenna space, $N_t = 4$, $N_a = 2$, $m = 2$, QPSK.	11
2.3	Simulation parameters.	17
3.1	Size of the search space for different values of N_a and m	31

List of Abbreviations

ABER	Average bit error rate
AP	Access point
bpcu	Bits per channel use
BS	Base station
CSMA/CA	Carrier sense multiple access with collision avoidance
DIFS	Distributed inter-frame space
DoA	Direction of arrival
DP	Dual-polarized
ES	Exhaustive search
ESM	Enhanced spatial modulation
FDMA	Frequency division multiple access
GSM	Generalized spatial modulation
G-SSK	Generalized space shift keying
IAI	Inter antenna interference
i.i.d	Independent and identically distributed
IoT	Internet of things
ISM	Industrial, Scientific and Medical
LAA	License-assessed access
LBT	Listen before talk
LLR	Log-likelihood ratio
LOS	Line of sight
LTE	Long term evolution
MIMO	Multiple-input multiple-output
ML	Maximum likelihood
MMSE	Minimum mean square error
MRC	Maximum ratio combining
NLOS	Non line of sight
NOMA	Non-orthogonal multiple access

OMA	Orthogonal multiple access
PA	power amplifier
PDMA	Pattern division multiple access
QoS	Quality of services
QSM	Quadrature spatial modulation
RF	Radio frequency
SIC	Successive interference cancellation
SM	Spatial modulation
SMX	Spatial multiplexing
SNR	Signal to noise ratio
SSK	Space shift keying
TDMA	Time division multiple access
TITO	Two-input two-output
UE	User equipped
U-NII	Unlicensed National Information Infrastructure
UP	Uni-polarized
Wi-Fi	Wireless fidelity
WLAN	wireless local area networks
XPD	Cross-polar discrimination
ZF	Zero forcing

Chapter 1

Introduction

1.1 Overview of Promising Communication Technologies

It has been known that communication industry is the main leading industry for future life. According to statistics [6], the global spending of this industry is estimated to approach 1428.9 billion U.S. dollars in 2018 and it keeps increasing even more in future. Applications of such an industry demand for wide range of requirements from high speed video streaming and augmented reality to low-data/power-limited internet of things (IoT) devices and health-care services. Obviously, providing such a diverse quality of service (QoS) including high speed, low data rate, enhanced reliability and coverage neither can be achieved with the current wireless infrastructure, nor by redesigning a single entity in mobile communication systems. Instead, it can be achieved solely based on combination of several advanced transmission technologies.

To address the high data rate-centric demands, novel technologies such as small-cell communication, densification, massive multiple-input multiple-output (MIMO) communication, and millimeter wave communication have become the roadmap for telecommunication industry and new standardizations [7].

Nevertheless, there are some bottlenecks in aforementioned technologies that make their deployment to be challenging. The main challenges arise as a result of space limitation, power restraint, and spectrum scarcity.

1.2 Thesis Motivation

As mentioned in the previous section, limited space, available power, and spectrum scarcity are the main limitations in communication systems. As an example, massive MIMO is realized by placement of the large number of antennas (in order of hundreds). Nevertheless, positioning of these antennas together with all their analog elements (such as phase shifters and power amplifiers) is subject to violate the cost and power limitation. On the other hand, packed antenna implementation creates spatial correlation and degrades the performance of transmission. Therefore, it is necessary to design a new transmission strategy with reduced radio frequency (RF) chain while providing a reasonable data rate.

Another problem that arises with large number of antennas is energy consumption. To be specific, every antenna element is accompanied by a RF chain and thus, increasing number of antennas requires more RF chains. Moreover, each RF chain contains power amplifier (PA). Considering the fact that 70% of the total energy in a base station (BS) is consumed by PA and dissipated as heat [8], novel hardware design is a vital factor from energy/power efficiency point of view. The significant of new power efficient technology with limited number of RF chains becomes even more critical for applications such as low-power wearable and IoT devices. For these reasons, designing a new transmission approach with sufficient trade-off between number of RF chains and data rate needs to receive close study.

Spectrum scarcity is another limiting factor of future densified networks. One approach to deal with this problem is to share the spectrum, which can be realized in either licensed or unlicensed band. Spectrum sharing in licensed band has been widely studied under the main category of horizontal and vertical sharing [9]. In horizontal spectrum sharing, entities have the same priority while in vertical sharing, the secondary user has lower priority in comparison with the primary user. Seeking the additional spectrum has further led to idea of benefiting unlicensed band and offloading part of the long term evolution (LTE) data to the underutilized unlicensed spectrum. Considering the fact that 2.4 GHz Industrial, Scientific and Medical (ISM) and 5 GHz Unlicensed National Information Infrastructure (U-NII) bands are utilized by low-power wireless local area networks (WLAN) enabled devices, shifting LTE to unlicensed spectrum requires the new strategy to create an efficient coexistence between the two networks.

Another approach to cope with the resource scarcity and support the high traffic demand is to create an overlap in the resources assigned to different users. In the conventional multi-user techniques, orthogonal resources (non-overlapping resources) are assigned to different users and thus the interference has been eliminated. Evidently, the number of users that can be served is limited to the amount of resources. To address this restriction, a new direction of study, namely non-orthogonal multiple access (NOMA) has become of broad and current interest. Thanks to non-orthogonality aspect of NOMA, the number of users can be enlarged regardless of available resources. It is worth mentioning that the space and power constraints as explained earlier are even more emphasized in user ends, which highlights the significance of new energy efficient transmission scheme which can be applied to users under NOMA transmission.

1.3 Thesis Objectives

The main objective of this thesis is to study the aforementioned challenges and difficulties of next generation of wireless communication systems and develop novel approaches to alleviate these problems. To be more specific, we aim to

- Design and evaluate a compact implementation of MIMO systems and reduce the number of RF chains. Implementation of such a compact and energy efficient system is vital in many applications specifically in low-power devices such as wearable devices and IoT applications.
- Develop a spatially and efficient strategy for the coexistence of wireless fidelity (Wi-Fi) and LTE networks in unlicensed band which barely depends on modification in the current network infrastructure and protocols. In particular, we consider the interference reduction of one network on the other one to provide a cost-effective concurrent networks environment.
- Improve the network capacity with NOMA and for limited-power users who have constraint on the number of RF chains. It is crucial to achieve a sufficient capacity with minimum number of RF chains. In essence, we aim to enhance the transmission capac-

ity by assigning the overlapped resources to the users while preserving the requirement of energy-efficient single RF chain.

1.4 Technical Contributions of the Thesis

The main contribution of the thesis is as follows:

- In Chapter 3 we propose a novel two-stage optimum antenna grouping scheme in generalized spatial modulation (GSM) with dual-polarized (DP) antennas. In the first stage of the proposed scheme, we select antennas with their polarizations as group indicators followed by the second stage, which determines the potential antennas and polarizations that can be selected within each group. The proposed algorithm directly chooses the activated antennas and therefore, completely eliminates the necessity of search over an extensive space.
- In Chapter 4, we propose to use the space dimension and beamforming to facilitate the effective coexistence and inter-network coordination. Two distinct approaches to evaluate the proposed coexistence mechanism, namely, Wi-Fi received power minimization and LTE user signal to noise ratio (SNR) maximization, have been investigated. The two proposed algorithms are simulated to show the potential and effective feasibility of coexistence between Wi-Fi and LTE in unlicensed spectrum.
- Chapter 5 focuses on multi-user scenario. We consider the uplink transmission where each user is constraint with single RF chain due to the space consideration. We implement the non-orthogonal multiple access to enhance the network capacity. Doing so, we first, analyze the performance of SM-based uplink NOMA transmission. Moreover, we propose a capacity-based pairing strategy for users with SM transmission.

1.5 Scope of Thesis

The rest of this dissertation is organized as follows:

The concept of SM (which is the fundamental building block for rest of the thesis) has been discussed in Chapter 2 followed by literature survey. After that, various detection algorithms have been introduced (including zero forcing (ZF), minimum mean square error (MMSE), successive interference cancellation (SIC), maximum likelihood (ML), and log-likelihood ratio (LLR)). At the end of the Chapter, performance analysis of SM with different detection algorithms (together with their advantages and disadvantages) have been discussed.

In Chapter 3 we study the benefit of antenna selection in SM-MIMO system. In addition, we consider two orthogonal polarization (whose dimension is twice the virtual system with uni-polarized antennas) to make a compact deployment. Utilizing dual-polarized antenna elements is a promising solution to the problem of space limitation in MIMO system while creating a sufficient inter-antenna correlation. Such a compact implementation is even more favorable in scenarios when the number of antennas increases as in the case of massive MIMO.

In Chapter 4, we take advantage of inherent aspect of LTE and Wi-Fi networks, i.e., multiple antennas, to steer the beam into the desired direction and thus alleviate the inevitable impact of LTE deployment in unlicensed band on the performance of Wi-Fi operators. To be more specific, we start with the system model including the coexistence of networks and optimize the beamforming weights in two different approaches, namely Wi-Fi received power minimization and LTE user SNR maximization.

In Chapter 5, we investigate the uplink transmission with NOMA for the users with limited number of RF chains. In particular, we consider the users utilizing SM and we apply the successive interference cancellation to detect the message. After that, we look into the achievable sum rate capacity of the SM-NOMA as a criteria to study the effect of pairing in SM-NOMA.

Chapter 2

Principle and Detection Analysis of Spatial Modulation

2.1 Modulation in Space Domain

In communication systems, the characteristics of a signal does not, by nature, match the characteristics of channel. That is why a transmitted signal is preprocessed before being conveyed, so that it meets the essential properties of the channel. Modulation, is a process of modifying signal such that it can be fit to channel. Conventionally, there are three main features of the signal that can be exploited to carry different information resulting in the following modulation schemes:

- Frequency modulation (FM)
- Amplitude modulation (AM)
- Phase modulation (PM)

Accordingly, in MIMO communication, every signal corresponding to a particular antenna is being modulated individually. Nevertheless, MIMO systems are suffering from certain challenges, such as inter antenna interference (IAI), and synchronization error. Another difficulty in MIMO communication is related to number of RF chains. On one side (depending on the application and/or for economical and environmental reasons), there may not be enough space

for large number of RF chains. On the other side, each RF chain contains a power amplifier, which is the most power hungry component of the circuit. Therefore, increasing number of RF chains is prohibitive as it reduces the energy efficiency of the system, which is vital for low-power applications such as in IoT devices.

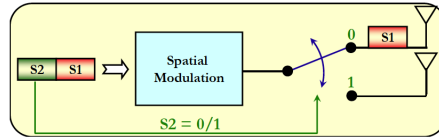
In order to address these challenges while benefiting from space dimension, new modulation scheme is required for the next generation of wireless communication systems. One promising solution, which have become of broad and current interest, is known as index modulation. One approaches to implement index modulation is to solely utilize the antenna index (instead of signal itself) for the sake of information conveyance. This method is known as space shift keying (SSK) modulation [10], where the input bit stream enters into SSK mapper and works as a switch between transmit antenna elements. In other words, only a single antenna is used at any particular transmission instance to propagate the power and rest of the antenna elements are de-active. More general form of SSK is proposed in [11] and is well-known as generalized SSK (G-SSK) modulation. In this G-SSK, N_a antennas are simultaneously activated to propagate the power.

While SSK and G-SSK benefit from simple and low-cost implementation, they suffer from low data rates. Therefore, in order to increase the spectral efficiency, the active antennas at SSK and G-SSK can be deployed to transmit a conventional constellation symbol. The idea of transmitting a symbol constellation from single active antenna is proposed by Mesleh *et al.* [12], which is recognized as spatial modulation (SM).

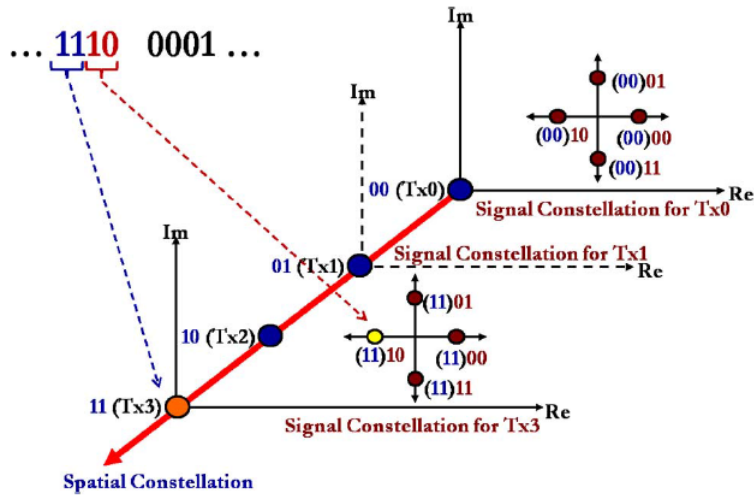
2.1.1 Spatial Modulation Technique

As mentioned earlier, unlike SSK modulation, where input bits operates as a switch to select an antenna, in SM the input bit stream is divided into two portions as shown in Fig. 2.1a by S1 and S2. Throughout the transmission, one part, say (S2), is used to switch between antennas, i.e., assuming two transmit antennas, first and second antenna is switched on when S2 is zero and one, respectively. Subsequently, the other part of data stream (S1) is mapped to the constellation space, which will be further transmitted by the activated antenna.

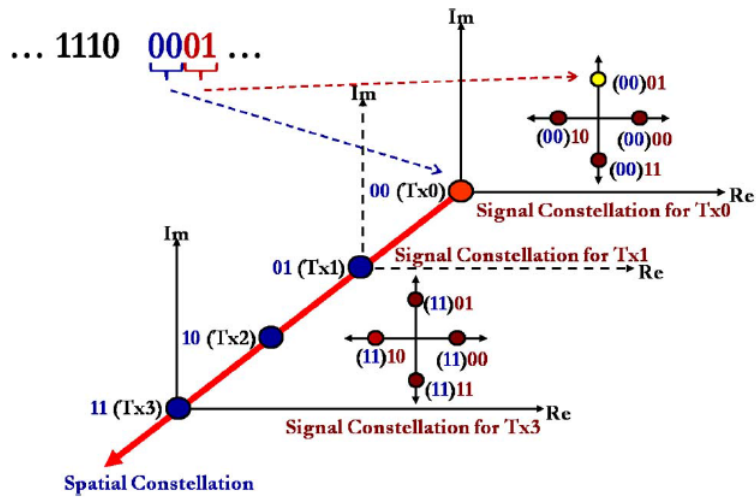
Fig. 2.1b is an example of SM-MIMO system with 4 transmit antennas conveying a QPSK



(a) Using part of an input stream to switch between transmit antennas.



(b) Constellation symbols transmitted over different antennas at first transmission instant.



(c) Constellation symbols transmitted over different antennas at second transmission instant.

Figure 2.1: Illustration of SM transmission algorithm [1].

Table 2.1: SM scheme, Mapping input bits to corresponding constellation symbols and antenna space.

Incoming bits	Symbol bits	Antenna	\mathbf{x}^T	X_s
$\underbrace{0\ 0}_{\text{symbol bits}}\ \underbrace{0\ 0}_{\text{antenna}}$	00	1	$[0\ 0\ 0\ 1]$	1
0001	00	2	$[0\ 0\ 1\ 0]$	1
0010	00	3	$[0\ 1\ 0\ 0]$	1
0011	00	4	$[1\ 0\ 0\ 0]$	1
0100	01	1	$[0\ 0\ 0\ j]$	j
0101	01	2	$[0\ 0\ j\ 0]$	j
0110	01	3	$[0\ j\ 0\ 0]$	j
0111	01	4	$[j\ 0\ 0\ 0]$	j
1000	10	1	$[0\ 0\ 0\ -1]$	-1
1001	10	2	$[0\ 0\ -1\ 0]$	-1
1010	10	3	$[0\ -1\ 0\ 0]$	-1
1011	10	4	$[-1\ 0\ 0\ 0]$	-1
1100	11	1	$[0\ 0\ 0\ -j]$	$-j$
1101	11	2	$[0\ 0\ -j\ 0]$	$-j$
1110	11	3	$[0\ -j\ 0\ 0]$	$-j$
1111	11	4	$[-j\ 0\ 0\ 0]$	$-j$

constellation symbol. This example requires two bits of input for the spatial domain and another two bits for the constellation symbol (which results in transmission of 4 bits at each transmission time). For the sake of illustration, assume the input bits in a particular transmission instant is 1110. Such an input can be further divided into 11 and 10 (as explained before). The first part (11) is mapped to the antenna space and thus it activates the fourth antenna, which is shown by color red. Notice that rest of the antennas are silent. The second part of the input bits (10) is assigned to the constellation diagram, which correspond to the third symbol in QPSK and is highlighted by color yellow in the Figure. As a result, the constellation symbol corresponding to input 10 is transmitted over fourth antenna element.

Alternatively, Fig. 2.1c gives an example of another transmission instance, when the input bits are assume to be 0001. The aforementioned SM mapping strategy is tabulated in Table 2.1.

2.1.2 Multi-stream Generalized Spatial Modulation

As in the case of SSK and G-SSK, SM can be generalized to trigger $1 < N_a < N_t$ antennas and transmit more than one symbol at a given transmission attempt. As such, generalized spatial modulation (G-SM) takes the advantages of conventional SM as well as benefiting from diversity gain. It worth mentioning that, deciding on an appropriate number of active antennas (N_a) is an important factor as it brings a trade of between complexity and data rate. For the purpose of illustration, notice that there are $\binom{N_t}{N_a}$ different combinations to select N_a antennas from the total N_t transmitters. On the other hand, considering m bits to select a set of antennas containing N_a elements results in 2^m choices, which causes $\binom{\binom{M}{N_a}}{2^m}$ distinct options. As an example, consider a system with 4 transmit antennas out of which only 2 active antennas are required. Furthermore, assume $m = 2$. In such an example, there exists $\binom{4}{2} = 6$ sets including two antennas among which only $2^m = 2^2 = 4$ sets can be used for the transmission. This results in $\binom{6}{4} = 15$ different combinations. Notice that, increasing the number of transmit antennas dramatically enlarges the number of combinations, each with different performance [13]. Therefore, to address the challenge of selecting the optimum set of antennas by a feasible approach, that eliminates the exhaustive search over entire set of combinations, is vital and subject of the next Chapter.

An example of G-SM bit mapping strategy from input bits to antenna space and symbol constellation is tabulated in Table 2.2. In this example, two activated antennas out of four transmit antennas are used to convey a QPSK symbol.

In addition to enhanced spectral efficiency, G-SM has another advantage over SM transmission. Particularly, unlike SM, where number of transmit antennas has to be a power of two, G-SM does not have any constraint in this regard.

In addition to SSK/G-SSK and SM/G-SM, there are other methods to spatially modulate the signal while increasing the spectral efficiency. Examples of these methods are quadrature spatial modulation (QSM) and enhanced spatial modulation (ESM). It is also worth mention-

Table 2.2: G-SM scheme, Mapping input bits to corresponding constellation symbols and antenna space, $N_t = 4$, $N_a = 2$, $m = 2$, QPSK.

Incoming bits	Symbol bits	Antennas	\mathbf{x}^T	X_s
$\overbrace{0\ 0}^{\text{symbol bits}}\ \overbrace{0\ 0}^{\text{antenna index}}$	00	(1,2)	$\frac{1}{\sqrt{2}} \begin{bmatrix} 1 & 1 & 0 & 0 \end{bmatrix}$	1
0001	00	(3,4)	$\frac{1}{\sqrt{2}} \begin{bmatrix} 0 & 0 & 1 & 1 \end{bmatrix}$	1
0010	00	(2,3)	$\frac{1}{\sqrt{2}} \begin{bmatrix} 0 & 1 & 1 & 0 \end{bmatrix}$	1
0011	00	(4,1)	$\frac{1}{\sqrt{2}} \begin{bmatrix} 1 & 0 & 0 & 1 \end{bmatrix}$	1
0100	01	(1,2)	$\frac{1}{\sqrt{2}} \begin{bmatrix} j & j & 0 & 0 \end{bmatrix}$	j
0101	01	(3,4)	$\frac{1}{\sqrt{2}} \begin{bmatrix} 0 & 0 & j & j \end{bmatrix}$	j
0110	01	(2,3)	$\frac{1}{\sqrt{2}} \begin{bmatrix} 0 & j & j & 0 \end{bmatrix}$	j
0111	01	(4,1)	$\frac{1}{\sqrt{2}} \begin{bmatrix} j & 0 & 0 & j \end{bmatrix}$	j
1000	10	(1,2)	$\frac{1}{\sqrt{2}} \begin{bmatrix} -1 & -1 & 0 & 0 \end{bmatrix}$	-1
1001	10	(3,4)	$\frac{1}{\sqrt{2}} \begin{bmatrix} 0 & 0 & -1 & -1 \end{bmatrix}$	-1
1010	10	(2,3)	$\frac{1}{\sqrt{2}} \begin{bmatrix} 0 & -1 & -1 & 0 \end{bmatrix}$	-1
1011	10	(4,1)	$\frac{1}{\sqrt{2}} \begin{bmatrix} -1 & 0 & 0 & -1 \end{bmatrix}$	-1
1100	11	(1,2)	$\frac{1}{\sqrt{2}} \begin{bmatrix} -j & -j & 0 & 0 \end{bmatrix}$	-j
1101	11	(3,4)	$\frac{1}{\sqrt{2}} \begin{bmatrix} 0 & 0 & -j & -j \end{bmatrix}$	-j
1110	11	(2,3)	$\frac{1}{\sqrt{2}} \begin{bmatrix} 0 & -j & -j & 0 \end{bmatrix}$	-j
1111	11	(4,1)	$\frac{1}{\sqrt{2}} \begin{bmatrix} -j & 0 & 0 & -j \end{bmatrix}$	-j

ing that non of the aforementioned spatial modulation techniques requires any channel state information at the transmitter.

In summary, deploying a MIMO system brings a number of challenges, some of which are itemized as follows and can be eliminated by spatial modulation techniques:

- Transmission of multiple bit streams requires the inter- antenna synchronization at the transceiver sides.
- Each RF chain consists of PA, which in turn is the most power hungry component of the system. Therefore, as the number of RF chain increases, the energy and power-efficiency decreases.
- Inter-channel interference, which is a result of conducting multiple antennas degrades the performance.

2.2 Detection Algorithms

While the benefits of MIMO systems are well known for the future communication systems, yet another difficulty of MIMO systems arises at the receiver side during the signal detection. In general, detection algorithms fall into two main categories, i.e., linear and non-linear detections, some of which are discussed in this Section.

2.2.1 Low-complex Suboptimal Linear Detection

Linear detection algorithms aim to detect all transmitted streams at once by reversing the effect of channel. Nevertheless, detection of all streams together reduces the diversity order.

Zero Forcing (ZF) Detection Algorithm

In ZF detection algorithm, the received signal is multiplied by inverse of the channel matrix to achieve

$$\mathbf{H}^{-1}\mathbf{y} = \mathbf{x} + \mathbf{H}^{-1}\mathbf{n}. \quad (2)$$

This equation can be further used to detect the transmitted signal \mathbf{x} . In other words, the weight matrix in ZF is defined as $W_{ZF} = \mathbf{H}^{-1}$. Notice that in some practical applications, different number of antennas are located at the transmitter and receiver. In such cases, the inverse of the channel matrix can be replaced by its pseudo-inverse and thus

$$W_{ZF} = (\mathbf{H}^H\mathbf{H})^{-1}\mathbf{H}^H. \quad (3)$$

It is also worth mentioning that, maximum ratio combining (MRC) approach is a spatial case of ZF. In particular, in scenarios, where there are single transmit antenna and multiple receive antennas, ZF reduces to MRC [2].

Minimum Mean Square Error (MMSE) Detection Algorithm

Considering the last term in (2), one can notice that when the channel is in deep fade, i.e., channel coefficients are close to zero, noise component enhances and deteriorates the performance of detection. Therefore, in order to alleviate noise enhancement, another approach has been proposed to find the weight matrix at the receiver side, which is based on minimizing the mean square error and can be written as

$$\begin{aligned}\mathbf{W}_{MMSE} &= \min_{\mathbf{W}} E \{ \|\mathbf{x} - \mathbf{W}\mathbf{y}\|^2 \} \\ &= \min_{\mathbf{W}} E \{ (\mathbf{x} - \mathbf{W}\mathbf{y})^H (\mathbf{x} - \mathbf{W}\mathbf{y}) \}.\end{aligned}$$

Taking the derivative of the above equation with respect to \mathbf{W} and set it to zero results in the \mathbf{W}_{MMSE} represented by

$$\mathbf{W}_{MMSE} = (\mathbf{H}^H \mathbf{H} + N_0 \mathbf{I})^{-1} \mathbf{H}^H. \quad (4)$$

2.2.2 Successive Interference Cancellation Detection

To further improve the detection performance with acceptable increase in complexity, a series of linear detection algorithms can be deployed in a multi-stream communication systems. In this approach, every stream is reduced from the received signal after being detected. This method is well-known as successive interference cancellation (SIC). For the sake of illustration, the block diagram of such an algorithm is shown in Fig. 2.2.

2.2.3 Optimal Maximum Likelihood Detection

Similar to SIC, maximum likelihood detection is a non-linear detection. Notice that likelihood function of received signal \mathbf{y} is defined as the following probability

$$P(\mathbf{y}|\mathbf{H}, \mathbf{x}) = \frac{1}{\sqrt{2\pi N_0}} e^{-\frac{\|\mathbf{y} - \mathbf{H}\mathbf{x}\|^2}{2N_0}}, \quad (5)$$

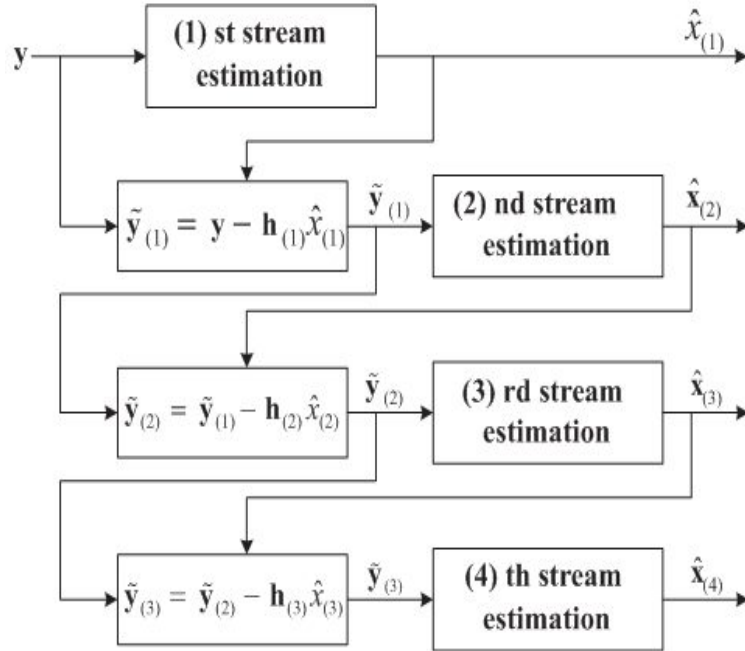


Figure 2.2: Successive interference cancellation approach [2].

in which N_0 is the variance of noise. To detect the transmitted signal, likelihood function needs to be maximized, which alternatively is equivalent to minimizing the following distance metric

$$\hat{\mathbf{x}} = \arg \min_{\forall \mathbf{x}} \|\mathbf{y} - \mathbf{H}\mathbf{x}\|^2, \quad (6)$$

for all possible constellation symbols.

Notice that although ML detection is computationally expensive (as it searches through all possible constellations) in comparison with linear detection algorithms, implementation of ML on SM (shown in Fig. 2.3) achieves lower complexity compared to ML detection in spatial multiplexing (SMX). To be more specific, MIMO-SM with ML detection has $200(N_t - 1)/(2N_t + 1)\%$ complexity reduction in comparison with ML detection in SMX with the same spectral efficiency [3]. That means 40% and more than 66% complexity reduction for systems with two and four transmit antenna elements, respectively.

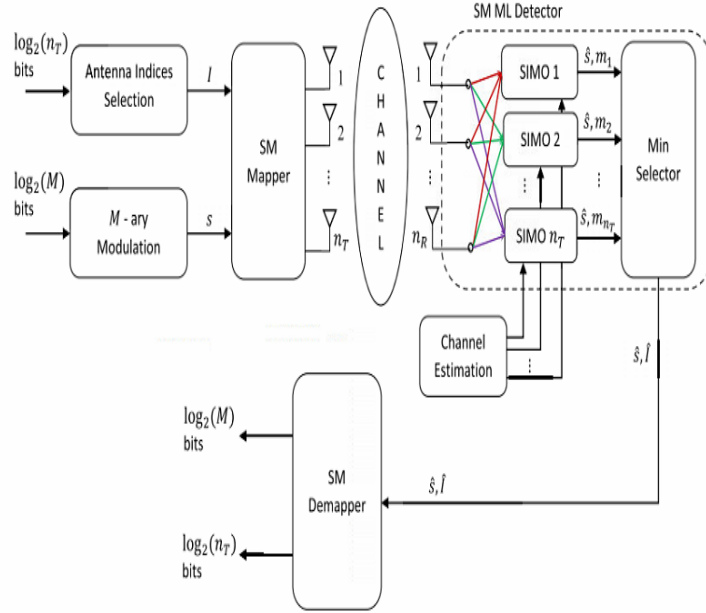


Figure 2.3: Block diagram of SM transmission and ML detection structure [3].

2.2.4 Log-Likelihood Detection Algorithm

The above mentioned detection algorithms are known as hard decision algorithms. Nevertheless, in order to reduce the information loss, other detection algorithms have been proposed based on soft information. An example of such an algorithm is log-likelihood ratio (LLR) [2].

In MIMO systems, it is convenient to deploy soft decision in two steps. In the first stage, a linear decoder is deployed to separate different bit streams, each of which can be further considered for LLR calculation. To illustrate, let us consider a received signal as

$$\begin{aligned} \mathbf{y} &= [\mathbf{h}_1 \cdots \mathbf{h}_{N_r}] \mathbf{x} + \mathbf{n} \\ &= \mathbf{h}_1 x_1 + \cdots + \mathbf{h}_{N_r} x_{N_r} + \mathbf{n}. \end{aligned} \quad (7)$$

Then, the received signal can go through the linear combination (using \mathbf{w}_i) to separate the i -th bit as

$$\begin{aligned} \hat{x}_i &= \mathbf{w}_i \mathbf{y} \\ &= \mathbf{w}_i \mathbf{h}_1 x_1 + \cdots + \mathbf{w}_i \mathbf{h}_i x_i + \cdots + \mathbf{w}_i \mathbf{h}_{N_r} x_{N_r} + \mathbf{w}_i \mathbf{n}. \end{aligned} \quad (8)$$

Notice that, as in the last Section, \mathbf{w}_i is i -th row of matrix \mathbf{W} corresponding to either MMSE or ZF. In (8), desired component, interference and noise component are

$$d_i = \mathbf{w}_i \mathbf{h}_i x_i, \quad (9)$$

$$I_i = \sum_{j=1, j \neq i}^{N_i} \mathbf{w}_i \mathbf{h}_j x_j, \quad (10)$$

and

$$n_i = \mathbf{w}_i \mathbf{n}, \quad (11)$$

respectively. In addition, considering independent noise and interference, the overall undesired signal is a zero mean Gaussian random variable with variance of

$$\sigma_i^2 = \sum_{j=1, j \neq i}^{N_i} |\mathbf{w}_i \mathbf{h}_j|^2 E\{|x_j|^2\} + \|\mathbf{w}_i\|^2 \sigma_n^2. \quad (12)$$

Therefore, the conditional probability of estimating the i -th symbol given the exact value is obtained by

$$f(\hat{x}_i | x_i) = \frac{1}{\sqrt{2\pi\sigma_i^2}} \exp\left(-\frac{|\hat{x}_i - d_i|^2}{2\sigma_i^2}\right). \quad (13)$$

Assuming L -ary modulation, each symbol contains $\log_2(L)$ bits. Notice that, considering a certain bit in i -th symbol, say l -th bit ($b_{i,l}$), the L -ary modulation space can be divided to two subsets, i.e., those with $b_{i,l} = 0$ and those with $b_{i,l} = 1$, which can be represented by $\mathcal{S}_{i,l}^0$ and $\mathcal{S}_{i,l}^1$. As such, the LLR corresponding to the l -th bit of i -th symbol can be evaluated as

$$LLR(b_{i,l}) = \ln \frac{\sum_{x \in \mathcal{S}_{i,l}^1} f(\hat{x}_i | x)}{\sum_{x \in \mathcal{S}_{i,l}^0} f(\hat{x}_i | x)}, \quad (14)$$

which can be approximated as

$$\begin{aligned}
 LLR(b_{i,l}) &\approx \ln \frac{\max_{x \in S_{i,l}^1} f(\hat{x}_i|x)}{\max_{x \in S_{i,l}^0} f(\hat{x}_i|x)} \\
 &= \frac{1}{2\sigma_i^2} \left(|\hat{x}_i - x_{i,l,Opt}^0|^2 - |\hat{x}_i - x_{i,l,Opt}^1|^2 \right), \tag{15}
 \end{aligned}$$

where

$$x_{i,l,Opt}^0 = \arg \min_{x \in S_{i,l}^0} |\hat{x}_i - x|^2, \tag{16}$$

$$x_{i,l,Opt}^1 = \arg \min_{x \in S_{i,l}^1} |\hat{x}_i - x|^2. \tag{17}$$

Based on above equations and for the sake of illustration, we consider a 2×2 MIMO system and evaluate the performance of LLR detection for different spectral efficiencies, namely, 8 bpcu and 4 bpcu. The results of Monte Carlo simulation is depicted in Fig. 2.5. We consider the convolutional code with coding rate of $1/2$, with block diagram shown in Fig. 2.4.

The channel is assumed to follow Rayleigh distribution and the Viterbi algorithm has been deployed at the receiver with trace-back length of 32. These parameters are summarized in the Table 2.3.

Table 2.3: Simulation parameters.

Parameter	Value
N_t	2
N_r	2
Coding rate	$1/2$
Coding scheme	Convolutional code
Trace back length for Viterbi algorithm	32
Polynomials	1111001=171(Oct) 1011011=133(Oct)

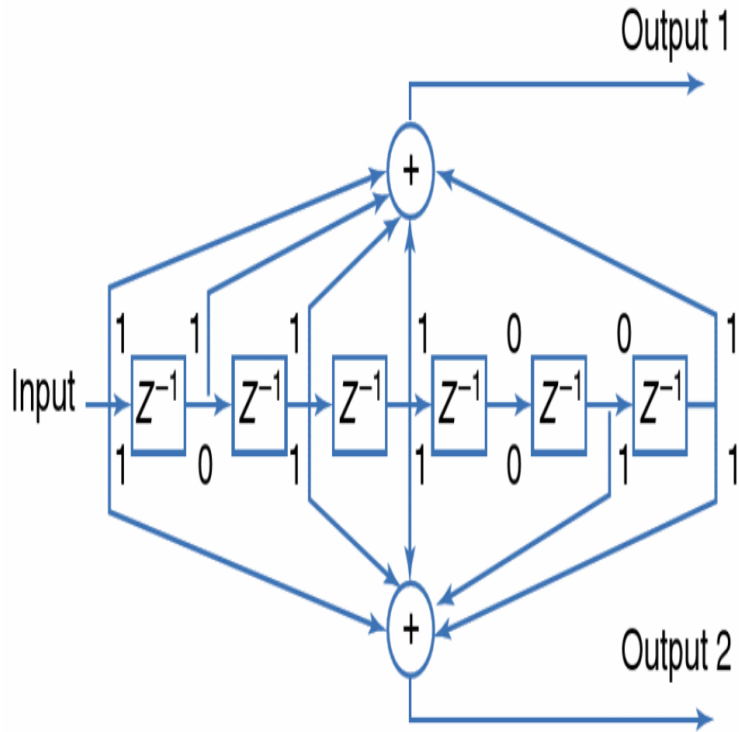


Figure 2.4: Convolutional encoder with coding rate of 1/2 [4].

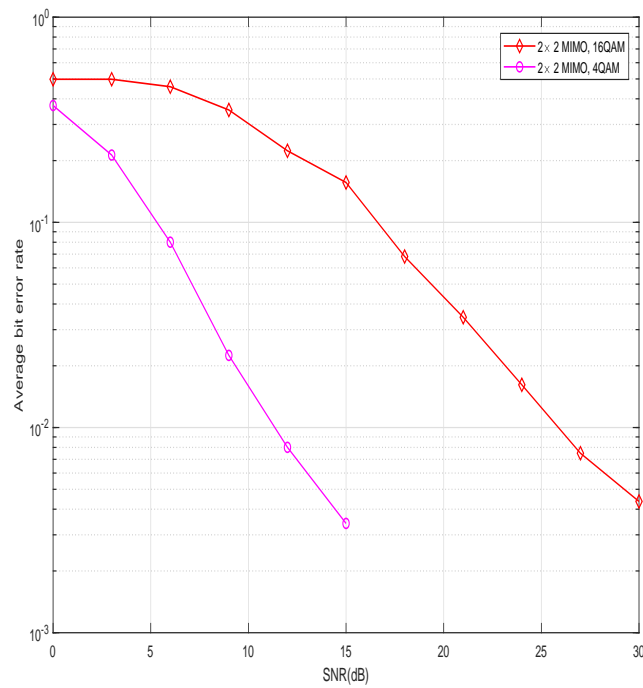


Figure 2.5: Performance analysis based on LLR detection.

2.2.5 Performance Analysis of SM with Different Detection Algorithms

As explained earlier, in SM, as opposed to the conventional MIMO systems, a single antenna is activated and the index of transmit antenna is used for the sake of information transmission. As a result, one RF chain is needed. Thanks to single RF chain requirement, energy efficient SM is a promising communication technology for future green transmission systems [1]. It is also worth mentioning that in conventional MIMO systems, number of receive antennas needs to be greater than those in transmitter, so that we can be able to apply MMSE or ZF. Nevertheless, as in the future wireless communication systems (such as in massive MIMO), where number of transmit antennas is dramatically larger than number of receive antennas (considering downlink), SM becomes more favorable [3]. In addition to energy efficiency, SM reduces the detection complexity. Maximum likelihood, which is known for its optimality and has been proposed in [14], reduces the detection complexity from $O(M^{N_t})$ in MIMO multiplexing to $O(MN_t)$ in SM (assuming N_t transmit antennas and constellation size of M). Other types of sub-optimal detection algorithms for SM-MIMO have been proposed, which further reduces the complexity. Among all suboptimal detection approaches, [15] has proposed the separate detection of the index information and symbol constellation and has become one of the most important approaches. This separation and the fact that only a single antenna is activated allows us to take advantage of simple MRC approach. As a result, the detection complexity reduces to $O(N_t + M)$.

In this section, we consider the performance of SM and compare the results with SMX transmission having the same spectral efficiency. Notice that in SMX different antennas transmit different bit streams and thus number of RF chains is equal to number of transmit antennas. Let us start with the optimum detection algorithm, i.e., ML detection. In SM, the receiver uses the ML to jointly detect the transmitted symbol as well as antenna indices.

We have made the comparison for different spectral efficiencies, i.e., $R=6$ and 10 bits per channel use (per subcarrier), which have been shown in Fig. 2.6 and Fig. 2.7, respectively. In SMX, we consider MIMO configuration with 2 antennas at the transmitter and receiver sides and the performance has been depicted with black line while different MIMO configurations for SM have been illustrated with colourful curves.

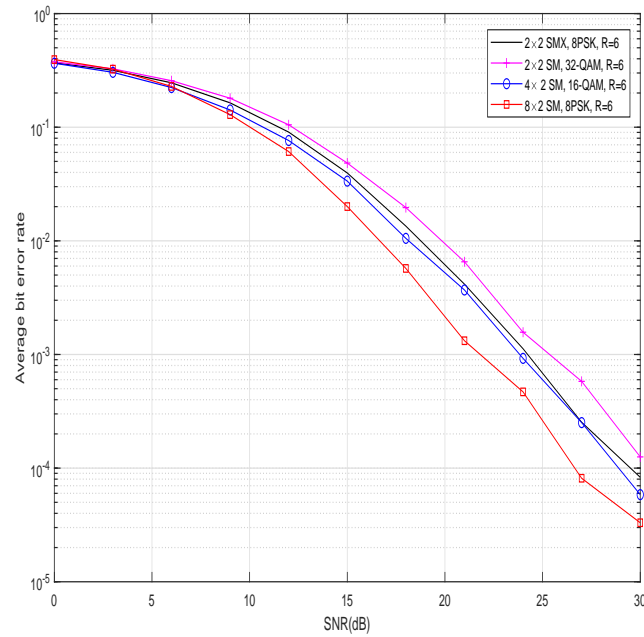


Figure 2.6: Comparison of spatial multiplexing and spatial modulation, 6 bits/subcarrier.

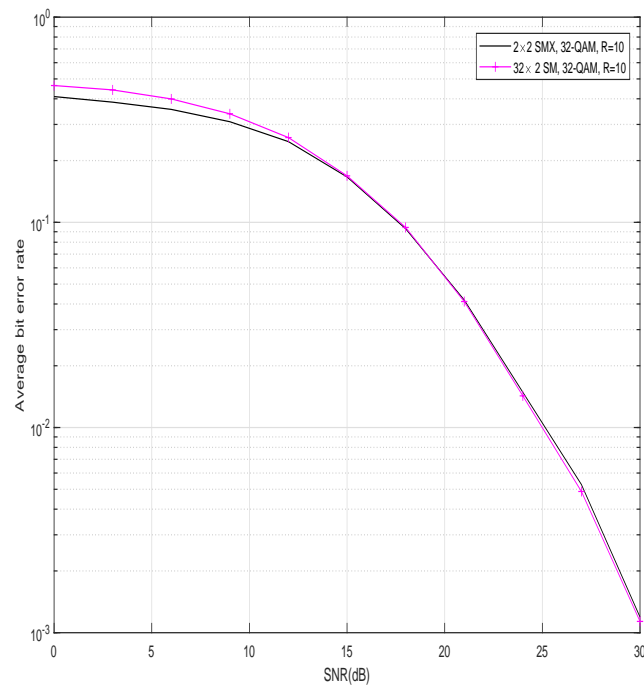


Figure 2.7: Comparison of spatial multiplexing and spatial modulation, 10 bits/subcarrier.

Considering spectral efficiency of 6, (Fig. 2.6), simulation results show that increasing the number of antennas, while utilizing a single RF chain, SM outperforms the MIMO system with SMX transmission. Likewise, for higher spectral efficiency, i.e., $R=10$ bpcu shown in Fig. 2.7, large number of antennas enables SM to achieve the performance of SMX while benefiting from low cost and power efficient implementation.

Fig. 2.8 shows the performance of SM in terms of ABER based on MRC detection and its comparison with ML algorithm. Notice that, in SM with MRC algorithm, detection of constellation symbols depends on the estimation of activated antenna index and thus if the antenna index is detected erroneously, the symbol estimation would be highly incorrect. This results can be seen in Fig. 2.8, where the joint detection of antenna index and symbol constellation, i.e., ML detection, outperforms the MRC approach.

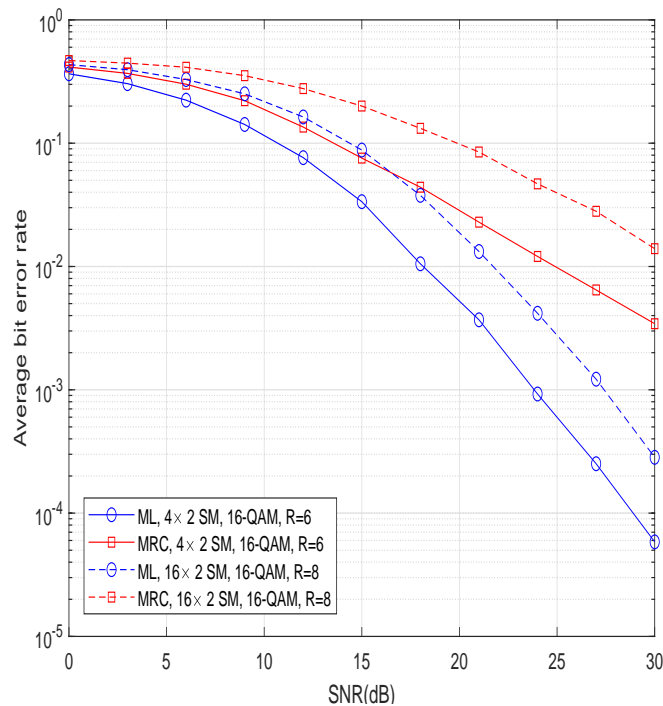


Figure 2.8: Comparison of MRC and ML detection of SM.

Finally, we have made the comparison of SM and SMX with LLR detection. Two different MIMO configurations are shown in Fig. 2.9 and Fig. 2.10. Comparing two aforementioned Figures, one can see that for the same spectral efficiency, increasing the number of antennas enables SM to outperform SMX.

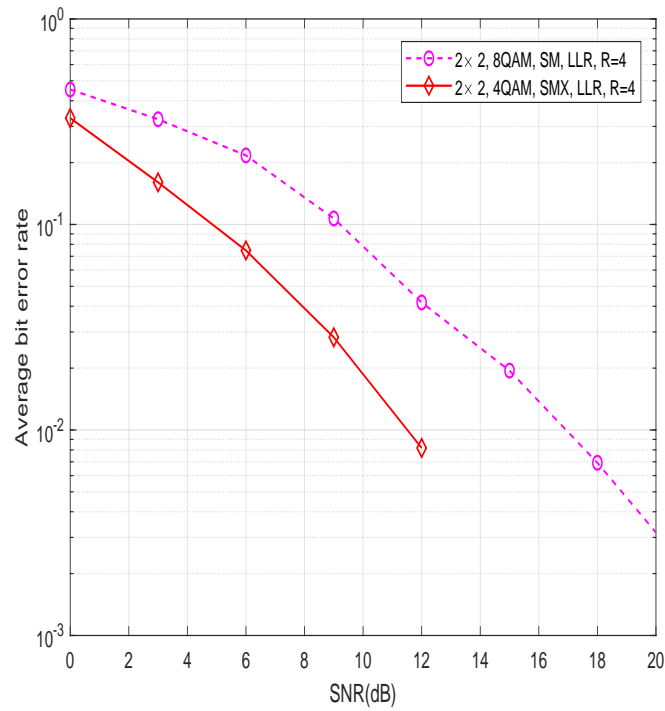


Figure 2.9: 2×2 SM-MIMO and SMX comparison based on LLR detection, $R = 4$.

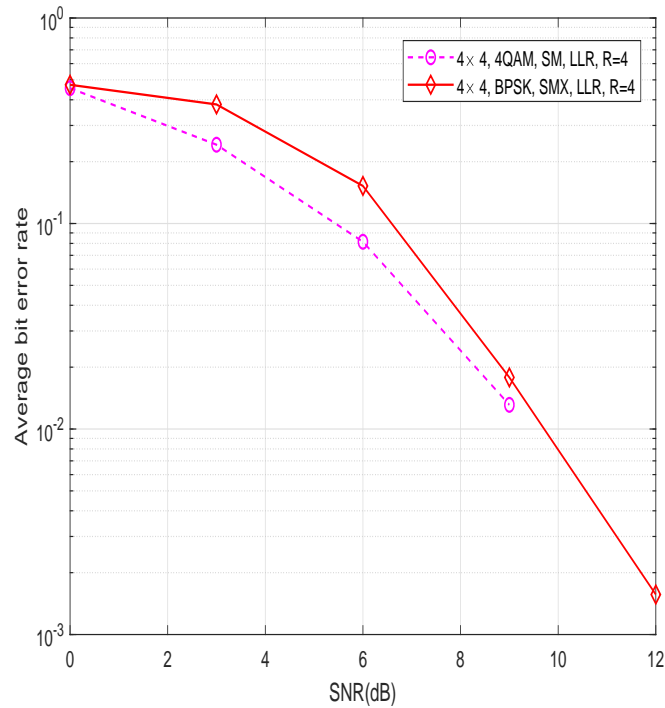


Figure 2.10: 4×4 SM-MIMO and SMX comparison based on LLR detection, $R = 4$.

Chapter 3

Antenna Selection in Dual-Polarized Generalized Spatial Modulation

3.1 Introduction

The anticipated 1,000 times of dramatic capacity increase in 5-th generation (5G) wireless networks has created many fundamental challenges. To meet the network capacity of 5G, massive multiple-input multiple-output (MIMO), which utilizes antenna array with a large number of elements, has been widely considered as a critical enabling technology for 5G due to its advantage of significantly increased spatial frequency reuse factor through the beamformed spatial transmission. However, the number of RF chains (which dominates the implementation cost of MIMO systems), needs to be equal to the number of antennas in conventional MIMO systems. Consequently, this requirement will drastically increase the implementation cost of massive MIMO systems due to a large number of antennas involved. As an alternative, spatial-modulation emerges as one promising solution to benefit from a large number of antennas while having limited number of RF chains, without sacrificing the data rate.

Spatial modulation (SM) is a relatively new transmission scheme, which uses the space dimension of antenna array to convey part of the bit stream to be transmitted [12]. In particular, part of the input bits is used to select an antenna to be activated while the other part is mapped onto the symbol that is transmitted through the selected antenna. Moreover, while SM is deployed over the MIMO systems, it uses only one activated antenna, which significantly

reduces the complexity of the transceivers.

During the recent years, SM is widely considered in literature and its potential benefits and challenges are evaluated [1]. The advantages of SM in large-scale MIMO systems is considered in [16]. In addition, the gain achieved by antenna selection in SM is addressed in [17] considering Euclidean distance and capacity of the system, while in [18], the authors use circle packing algorithm to maximize the minimum geometric distance between antennas to minimize the average bit error probability (ABEP) of SM-MIMO. Note that SM is a special case of generalized SM (GSM), where more than one antenna are used to convey the bit stream [19,20]. As indicated in [21], as the number of transmit antennas increases, GSM outperforms the conventional SM and therefore is preferable in massive MIMO. Nevertheless, the authors in [13] show that the performance of GSM varies depending on the different antenna grouping and not all of the antenna combinations benefit from sufficiently low ABEP. However, selecting an antenna group which results in the best performance using the exhaustive search is intractable. Therefore, to fill this gap, we present a novel and direct antenna grouping in GSM and remove the necessity of search.

On the other hand, the performance of GSM-MIMO systems deteriorates substantially with increased correlation among antennas due to insufficient inter-antenna spacing. In other words, to have adequate uncorrelated channels, antennas should be implemented in the order of half of the wavelength away from each other. However, by increasing the number of antennas in large-scale MIMO systems, this space requirement cannot be met with the space constraint of the transceivers. In addressing this, one promising approach to cope with the space limitation is to use dual-polarized (DP) antennas [22–26]. Two orthogonal polarizations can be utilized to differentiate the channels and impose an additional correlation due to the polarization mismatch. The aforementioned correlation is known as cross-polar discrimination (XPD) and its impact on the performance of antenna selection is considered in [27]. To take advantage of DP-MIMO, while exploring the space dimension and benefiting from the performance of the best antenna groups in GSM, we analyze a novel method to directly determine the optimum antenna groups in DP-GSM.

The overall contributions of this Chapter are as follows: We analyze a MIMO system deployed with DP antennas. Motivated by the circle packing antenna selection and considering

GSM scheme, we propose a two-stage algorithm to determine the optimum antenna groups and activate antennas within each group. In the first stage, we develop the procedure of selecting a representative antenna and its polarization for each group. In the second stage, we establish an algorithm to select antennas within each group to benefit from the advantages of GSM. We use the average bit error probability (ABEP) of the system to evaluate the performance of the proposed scheme and validate it by making a comparison with ABEP of the optimum antenna grouping in DP-GSM, which is obtained by the exhaustive search. In addition, we compare the performance of the proposed antenna grouping in DP-GSM system with the optimum performance of the system with uni-polarized (UP) antennas, whose number of antennas are twice as many as that of DP-MIMO.

The Chapter is organized as follows: In Section II, we introduce the system model and characteristics of the DP channel. The proposed algorithm on DP GSM is provided in Section III followed by the performance analysis in Section IV. We present the simulation results in Section V and conclude the Chapter in Section VI.

3.2 System Model

We consider a MIMO system with N_t and N_r DP antennas at transmitter and receiver, respectively, which leads to a $2N_t \times 2N_r$ dimensional channel between transmitter and receiver. We use N_t DP antennas to transmit $m + \ell$ bits at each transmission instance. Therefore, the spectral efficiency of such a system is $R = m + \ell$ bits per channel use (bpcu). In other words, at each transmission instant, $m + \ell$ bits are chosen from the incoming bit stream. ℓ bits are mapped onto the L -ary symbol space, where $L = 2^\ell$ and $\mathcal{X} = \{ X_1, \dots, X_k, \dots, X_L \}$ represents the set of constellation symbols. The other m bits are used to select one antenna group containing N_a antennas. In this work, we do not consider mapping optimization and therefore, both bit-to-antenna and also bit-to-symbol are uniformly mapped. Notice that the transmitted signal can be represented by a $2N_t \times 1$ vector $\mathbf{x}_{u,s}$, whose entries are 0 in all but N_a positions, which denote the indices of activated antennas in u th group. We assume that all N_a activated antennas transmit the same symbol $s \in \mathcal{X}$ and therefore, the values of all non-zero elements of transmit signal are the same and based on the selected modulation symbol. We assume there is a power

constraint of unity for transmitted signal, i.e., $E_x [\mathbf{x}_{u,s}^H \mathbf{x}_{u,s} = 1]$.

The transmit signal vector, $\mathbf{x}_{u,s}$, is then transmitted over a DP-MIMO channel and received by an array of $2N_r$ antennas as

$$\mathbf{y} = \frac{1}{\sqrt{N_a}} \mathbf{H} \mathbf{x}_{u,s} + \boldsymbol{\nu} \quad (1)$$

where division by $\sqrt{N_a}$ is for the purpose of power normalization. \mathbf{y} and $\boldsymbol{\nu}$ are the $2N_r \times 1$ vectors representing received signal and channel noise, respectively. The elements of $\boldsymbol{\nu}$ are independent identically distributed (i.i.d.) complex Gaussian variables with zero mean and variance N_0 , i.e., $\nu_k \sim \mathcal{CN}(0, N_0)$ for $k = 1, \dots, 2N_r$, thus signal to noise ratio (SNR) is defined by $SNR = \eta = \frac{E_s}{N_0} = \frac{1}{N_0}$. \mathbf{H} represents the $2N_r \times 2N_t$ channel matrix between transmitter and receiver whose elements are possibly correlated complex Gaussian random variables. Unlike uni-polarized antennas, correlation in MIMO channel with DP antennas includes the polarization effects within each DP antenna as well as spatial correlation due to the insufficient space between antennas. To shed lights on the impact of different correlation matrices, we first consider the single DP antenna at transmitter and receiver, which is also known as two-input two-output (TITO) system in the following subsection and exhibit the effect of polarization correlation. Consequently, we extend the TITO to MIMO scenario and present the impact of spatial correlation.

3.2.1 TITO Scenario

We consider a TITO system, where only one dual-polarized antenna is deployed at the transmitter and receiver. Therefore, the equivalent channel \mathbf{H} is a 2×2 matrix. If the channel is not rich enough to adequately distinguish different polarizations, the channel would be affected by the polarization correlation (XPC) between orthogonal polarization directions. However, as stated in [28], the polarization correlations are small can be ignored in calculations for the sake of simplicity. However, we consider it in our analytical derivations. The effect of polarization correlation in transmitter and receiver can be represented in matrix form as

$$\mathbf{\Pi}_t = \begin{bmatrix} 1 & \gamma_t \\ \gamma_t^* & 1 \end{bmatrix}, \quad \mathbf{\Pi}_r = \begin{bmatrix} 1 & \gamma_r \\ \gamma_r^* & 1 \end{bmatrix}, \quad (2)$$

respectively, where

$$\begin{aligned}\gamma_t &= \frac{E\{h_{i_p,i_p}h_{i_p,i_{p'}}^*\}}{\sqrt{\mu(1-\mu)}} = \frac{E\{h_{i_{p'},i_p}h_{i_{p'},i_{p'}}^*\}}{\sqrt{\mu(1-\mu)}}, \\ \gamma_r &= \frac{E\{h_{j_p,j_p}h_{j_p,j_{p'}}^*\}}{\sqrt{\mu(1-\mu)}} = \frac{E\{h_{j_{p'},j_p}h_{j_{p'},j_{p'}}^*\}}{\sqrt{\mu(1-\mu)}},\end{aligned}$$

and $0 < \mu \leq 1$ represents the amount of power leakage from one polarization to the other. In other words,

$$\mu = E\{|h_{i_p,i_{p'}}|^2\} = E\{|h_{i_{p'},i_p}|^2\}, \quad (3)$$

where $h_{i_p,i_{p'}}$ represents the channel coefficient between i th antenna with p th polarization and i th antenna with its orthogonal polarization, p' . Similarly, the rest of the power is expressed as

$$1 - \mu = E\{|h_{i_p,i_p}|^2\} = E\{|h_{i_{p'},i_{p'}}|^2\}. \quad (4)$$

The power ratio of co-polar to cross polar terms are characterized by XPD as described in [24] and shown by

$$\chi = \frac{1 - \mu}{\mu}. \quad (5)$$

The amount of XPD is proportional to the capability of the channel to distinguish between the two polarization directions.

3.2.2 MIMO Scenario

In this part, we consider the more general case with N_t and N_r DP antennas at the transmitter and receiver, respectively. Accordingly, the spatial correlation between antennas due to the insufficient spacing of antennas at transmitter and receiver can be represented in a matrix form, Σ_t and Σ_r , respectively. Notice that the correlation between separated antennas exponentially decreases as the geometrical distance between them increases. Therefore, the correlation

among i th and j th antenna can be calculated as in [18]

$$[\boldsymbol{\Sigma}_t]_{i,j} = \alpha_t^{d_{i,j}} \quad (6)$$

where $|\alpha_t| < 1$ and $d_{i,j}$ denotes the distance between i th and j th antennas.

Considering the effects of polarization correlation and spatial correlation, the generalized $2N_r \times 2N_t$ dual-polarized channel matrix can be written as [24]

$$\mathbf{H} = (\mathbf{1}_{N_r \times N_t} \otimes \boldsymbol{\Gamma}) \odot (\boldsymbol{\Psi}_r^{\frac{1}{2}} \mathbf{H}_w \boldsymbol{\Psi}_t^{\frac{1}{2}}) \quad (7)$$

where $\boldsymbol{\Gamma}$ is the leakage matrix which can be written as

$$\boldsymbol{\Gamma} = \begin{bmatrix} \sqrt{1-\mu} & \sqrt{\mu} \\ \sqrt{\mu} & \sqrt{1-\mu} \end{bmatrix}. \quad (8)$$

The operator \odot denotes the element-by-element Hadamard multiplication. \mathbf{H}_w is the size $2N_r \times 2N_t$ matrix modelling the fading part of the channel. The elements of \mathbf{H}_w are independent and identically distributed (i.i.d.), circularly symmetric zero mean complex Gaussian variables with unit variance. $\mathbf{1}_{N_r \times N_t}$ is an all one $N_r \times N_t$ matrix and \otimes denotes the Kronecker products. Finally, it can be shown that $\boldsymbol{\Psi}_r = \boldsymbol{\Sigma}_r \otimes \boldsymbol{\Pi}_r$ and $\boldsymbol{\Psi}_t = \boldsymbol{\Sigma}_t \otimes \boldsymbol{\Pi}_t$.

In order to adopt the antenna configuration as in [18], we assume the number of DP transmit antennas is a power of 2, i.e., $\log_2(N_t)$ is an integer. We assume the antennas are located in a square manner, where the number of antennas, A , in each edge of the square can be calculated as in [18] given by

$$A = \begin{cases} \sqrt{N_t} & \text{if } \log_2(N_t) \text{ is even} \\ 3 \times \sqrt{\frac{N_t}{8}} & \text{if } \log_2(N_t) \text{ is odd.} \end{cases} \quad (9)$$

Notice that when the $\log_2(N_t)$ is an odd number, $A_{\text{inner}} = \sqrt{\frac{N_t}{8}}$ antennas (located at the center of the square) are removed. Fig. 3.1 demonstrates the antenna configuration when number of DP antennas is 8 and 4, respectively,

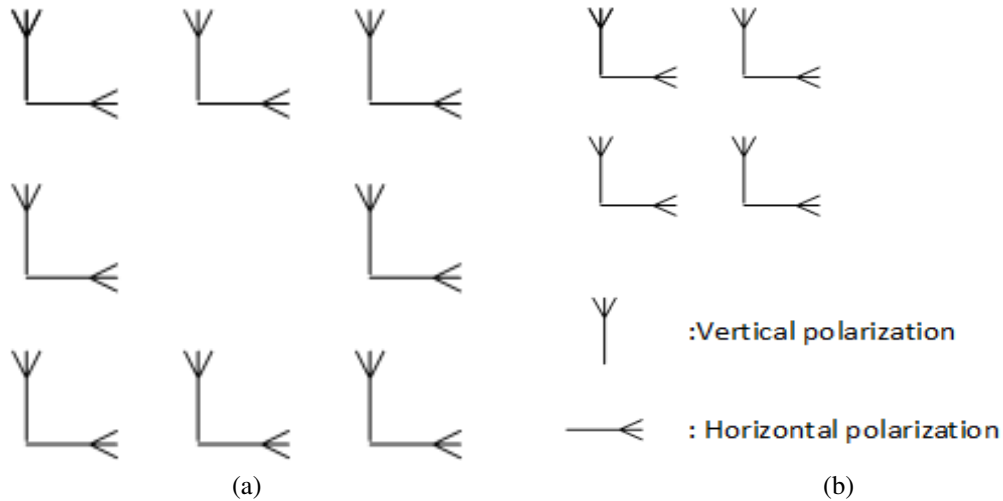


Figure 3.1: DP antenna configuration with different number of antennas, a) $N_t = 8$ DP antennas, b) $N_t = 4$ DP antennas.

3.3 Proposed Antenna Grouping

In this section, we present the antenna grouping in DP-GSM MIMO systems and deduce the framework to select N_a antennas within each group. In this regard, first we discuss the selection of antennas together with their polarization, which are representative of different group. Consequently, we consider the selection of N_a antennas within each group. Finally, the tractability of the algorithm is compared with exhaustive search over all possible combinations of antenna groups.

3.3.1 Selection of Group Indicators

Considering m bits to select a group containing N_a antennas as mentioned earlier, is equivalent to having 2^m groups of antennas. As stated in [18], the optimum performance in terms of ABEP can be achieved when these groups are chosen such that the correlation between them is low. Nevertheless, unlike the uni-polarized system in [18] and as stated earlier in Section II, MIMO systems with DP antennas are influenced not only by the spatial correlation but also by the polarization correlation. As the polarization correlation is usually low [28] and thus ignorable, the lowest correlations are among those antennas which have the most distance from each other in geometrical point of view, while having orthogonal polarizations. In order to be able to have the highest spatial distance, we consider the geometrical location of different groups

indicators to follow the circle packing algorithm as in [18]. However, notice that adjacent groups suffer from more spatial correlations. Therefore, to reduce the overall correlation we use different polarization from one group to its adjacent ones. For the sake of illustration, Fig. 3.2 presents an example of group's indicators (including antenna location and its corresponding polarization) by bold dashed lines. In this example, number of transmit DP antennas is 32, i.e., $N_t = 32$. In addition, we assume the number of bits assigned to select a group is 3 (i.e., $m = 3$), which is equivalent to $2^3 = 8$ groups of antennas.

3.3.2 Selection of Inner Group Antennas

Notice that there are N_a antennas to be activated within each selected group. Therefore, we suggest to select the N_a antennas in each group in such a way that they are highly correlated so that the overall correlation between different groups remains in its minimum level. Considering the fact that less spatial distance impose more spatial correlation among antennas and as arrays with similar polarizations are impacted by higher polarization correlation, we select N_a antennas within each group as those which are close in terms of geometrical distance while having the identical polarizations as those of the indicators. In Fig. 3.2 the activated antennas in each group are shown as solid bold lines. We assume, $N_a = 2$.

3.3.3 Feasibility of the Algorithm

In this Section, we evaluate the feasibility of the proposed algorithm and compare it with the size of search space when considering the exhaustive search to find the optimum groups of antennas to be activated. We illustrate the size of search space in exhaustive search via an example. Suppose there are N_t antennas at the transmitter and N_a activated antennas are used to convey the information symbols. Therefore, there are $\binom{N_t}{N_a}$ different combinations of antennas. In addition, m bits from input bit stream being mapped to the antenna space is equivalent to selection of 2^m groups of antennas out of the total $\binom{N_t}{N_a}$ groups. That results in

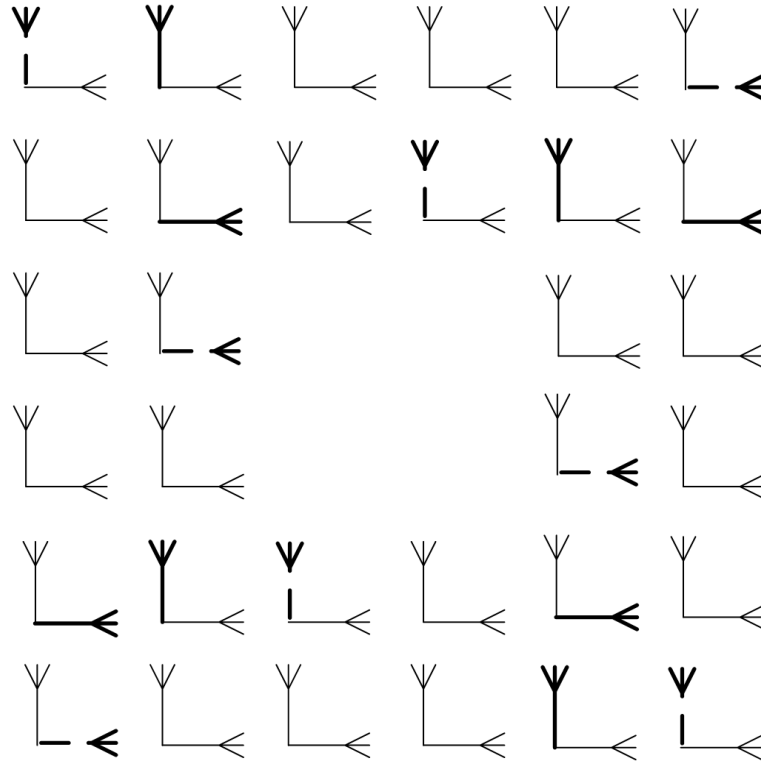


Figure 3.2: An example of antenna grouping considering their distance and polarizations, assuming $N_t = 32$ DP antennas, $m = 3$, and $N_a = 2$.

the search space of $\binom{\binom{N_t}{N_a}}{2^m}$ different combinations. Table 3.1 shows size of the search space when $N_t = 16$, and for different values of N_a and m .

$m \setminus N_a$	2	3
1	$\binom{\binom{16}{2}}{2} = 7140$	$\binom{\binom{16}{3}}{2} = 156520$
2	$\binom{\binom{16}{4}}{4} = 8214570$	$\binom{\binom{16}{4}}{4} > 4 \times 10^9$
3	$\binom{\binom{16}{8}}{8} > 8 \times 10^{11}$	$\binom{\binom{16}{8}}{8} > 8 \times 2^{17}$

Table 3.1: Size of the search space for different values of N_a and m .

As shown in Table 3.1, the search space dramatically increases as m and N_a become larger.

The large size of the search space in exhaustive search makes it intractable and highlights the importance of proposed scheme. Unlike in exhaustive search, the proposed method directly select the groups and antennas within each group together with their polarizations as explained in Section II (sub-section A and B) and illustrated in Fig. 3.2. Consequently, the proposed approach totally eliminates the search requirement.

Notice that $N_a = 1$ is a special case indicating the conventional spatial modulation. In such case, the proposed scheme reduces the dual-polarized version of the algorithm presented in [18] which still requires following the polarization switch from one activated antenna group to its adjacent groups.

3.4 Performance Analysis

To evaluate the accuracy of the proposed scheme, we consider the average bit error probability (ABEP) using the well-known upper bounding relation of [29] as

$$\bar{P}_b \leq \frac{1}{2^R} \sum_{u=1}^{2^m} \sum_{\hat{u}=1}^{2^m} \sum_{s=1}^L \sum_{\hat{s}=1}^L \frac{N(u, \hat{u}, s, \hat{s})}{R} \bar{P}_s(u, \hat{u}, s, \hat{s}) \quad (10)$$

where, R is the spectral efficiency as defined before. $N(u, \hat{u}, s, \hat{s})$ is the number of bits in error between the respective channel/polarization and symbol index pairs, and $\bar{P}_s(u, \hat{u}, s, \hat{s})$ is the corresponding average pairwise symbol error probability (APEP). Notice that each APEP is expressed as

$$\bar{P}_s(u, \hat{u}, s, \hat{s}) = E \left[Q \left(\sqrt{\frac{\|\mathbf{z}\|^2}{2}} \right) \right] \quad (11)$$

where $\mathbf{z} = \frac{1}{\sqrt{N_0 N_a}} (\mathbf{H} \mathbf{x}_{u,s} - \mathbf{H} \mathbf{x}_{\hat{u},\hat{s}})$. For the sake of simplicity in the analytical derivation, we alternatively represent the \mathbf{z} vector in vectorized form as

$$\begin{aligned} \mathbf{z} &= \frac{1}{\sqrt{N_0 N_a}} \Upsilon \text{vec}((\mathbf{1}_{N_r \times N_t} \otimes \mathbf{\Gamma})) \odot (\Psi^{\frac{1}{2}} \text{vec}(\mathbf{H}_w)) \\ &= \frac{1}{\sqrt{N_0 N_a}} \Upsilon \text{diag}\{\text{vec}((\mathbf{1}_{N_r \times N_t} \otimes \mathbf{\Gamma}))\} (\Psi^{\frac{1}{2}} \text{vec}(\mathbf{H}_w)) \end{aligned} \quad (12)$$

where $\Upsilon = (\mathbf{x}_{u,s} - \mathbf{x}_{\hat{u},\hat{s}}) \otimes \mathbf{I}$ and $\Psi = \Psi_l^T \otimes \Psi_r$. As stated in [13], it can be shown that \mathbf{z} forms a proper complex Gaussian random vector with its mean vector $\mathbf{0}$ and covariance matrix of Λ_z expressed as

$$\Lambda_z = \frac{1}{N_0 N_a} \Upsilon \Gamma' \Psi \Gamma'^{\dagger} \Upsilon^{\dagger} \quad (13)$$

where $\Gamma' = \text{diag}\{\text{vec}(\mathbf{1}_{N_r \times N_t} \otimes \Gamma)\}$ and $\text{diag}\{\cdot\}$ represents a diagonal matrix. As given in [30], the APEP in (9) can be computed by

$$\bar{P}_s(u, \hat{u}, s, \hat{s}) = \frac{1}{\pi} \int_0^{\frac{\pi}{2}} \left| \frac{\Lambda_z}{4 \sin^2 \theta} + \mathbf{I} \right|^{-1} d\theta. \quad (14)$$

Once each APEP term is computed via (14) the ABEP in (10) can be obtained conveniently.

3.5 Simulation Results

In this section, we present simulation results to evaluate the performance of the proposed antenna grouping scheme in DP-GSM systems. To this end, we consider the derived ABEP in the last Section. We assume $N_t = 8$ and $N_r = 1$ DP transmit and receive antennas, respectively. we assume $\gamma = 0.1$, as larger values usually are not considered [24]. All Figures provide the simulations for the scenarios when there are low and high spatial correlations among transmit antennas. In all Figures, two sets of curves represent the performance of the system with low spatial correlation between transmit DP antennas (depicted by the solid lines) and the highly correlated DP antennas at the transmitter (dashed lines). In all simulations, we assume $\alpha_t = 0.1$ for low spatial correlation and $\alpha_t = 0.8$ when the transmit DP antennas are highly correlated. In all Figures and for both set of curves, we compare the performance of the proposed algorithm and compare it with the best and the worst performances, which are obtained based on exhaustive search. Thus for the sake of comparison and to achieve antennas which result in the best and worst ABEP performances, we have evaluated the analytical derivations at a fixed SNR, i.e., SNR=30 dB and consider exhaustive search (ES) over all possible antenna groups. To this end and to be able to do the comparison, i.e., to make the exhaustive search tractable(without loss of generality), we consider 2 groups of antennas, i.e., $m = 1$.

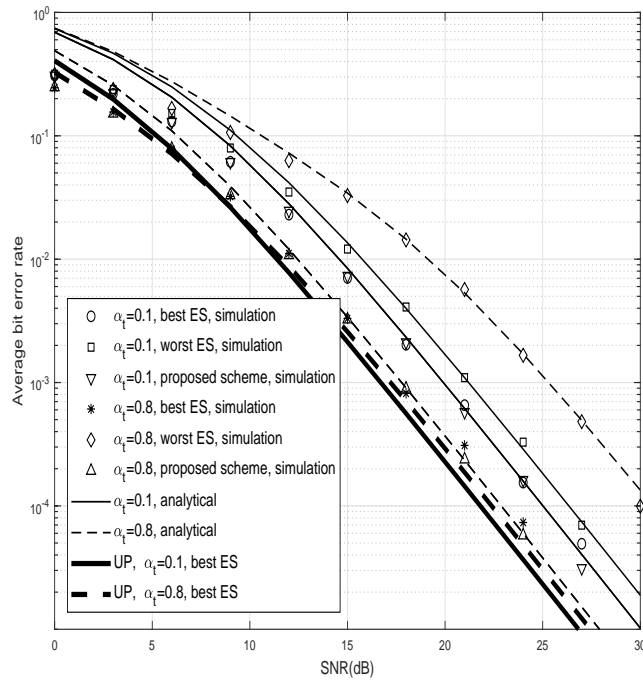
In Fig. 3.3 we assume two antennas are used ($N_a = 2$) to transmit a QPSK and 8-PSK symbols in different subfigure, i.e. $R = 3$ and 4 bpcu in part *a* and *b*, respectively. Likewise, in Fig. 3.4, we consider 3 activated antennas ($N_a = 3$) conveying QPSK and 8-PSK constellations in part *a* and *b*, respectively. The results indicate the tight match of the proposed antenna grouping algorithm with the best performance. All simulated performances are compared with the ABEP upper bounds; in the Figures, the simulated BER results are depicted only with the markers while the ABEP upper bounds are plotted with lines.

In addition, we compare the proposed method in DP-MIMO with the best performance of the equivalent channel with uni-polarized (UP) antenna elements. We use exhaustive search to find the antenna groups which results in the best ABEP. Notice that the number of physical channels in $N_t \times N_r$ DP-MIMO is equivalent to the those of the system with $2N_t \times 2N_r$ uni-polarized (UP) arrays. More specifically, we evaluate the performance of 16×2 UP-MIMO and compare it with 8×1 DP-MIMO. Notice that, since we consider the same antenna configuration as in [18], 16 UP antennas occupies 4/3 more space in each edge of the square. In other words, each edge contains 4 antennas in UP scenario while 3 DP antennas in DP-MIMO systems. We make the comparison in both cases of low and high correlated antennas. The performance of the UP-MIMO in Fig. 3.3 and Fig. 3.4 are depicted by bold lines. Notice that low and high correlations between antennas indicate the inter-antenna spacing is large and small, respectively.

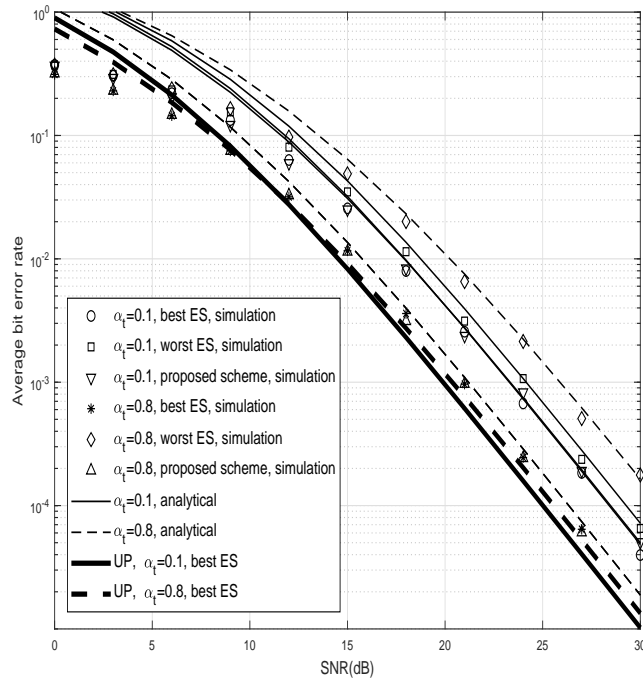
As shown in the Figures, in low correlation channels, DP-GSM suffers for about 3 dB performance loss while benefiting from the compact implementation. The advantages of DP-GSM is more highlighted in high correlated channels. Notice that in practice, antennas are implemented closed to each other (due to the space limitation), which impose higher correlation between antennas. In this scenario, DP-GSM reaches the performance of UP-GSM and yet take the advantage of close-packed deployment. These observations together with search elimination to find the optimum antenna groups highlights the importance of the direct antenna grouping method in DP-GSM.

3.6 Conclusion

In this Chapter, we use antenna polarization to differentiate different channels while achieving compact implementation of wireless transceivers with multiple antennas. We propose a two-stage antenna grouping scheme in generalized spatial modulation MIMO systems with dual-polarized antennas, which leads to the lowest possible ABEP (optimum performance). This algorithm directly selects the groups and activated antennas within each group, thus eliminating the requirement of searching for the groups with the best ABEP performance. The ABEP performance of the proposed algorithm is validated by Monte Carlo simulations. We also compare the ABEP of the proposed antenna grouping in DP-GSM with the optimum antenna groups which are obtained by exhaustive search and the results from the two methods are tightly matched. In addition, the simulation results validate the importance of the algorithm to optimally group the antennas in DP-GSM as compared to UP-GSM. In particular, when the channel is high correlated, the proposed method for DP-GSM reaches the optimum performance of the UP-GSM with a twice as many as antennas in DP-MIMO. In low correlation channels, DP-GSM is preferable in terms of physical space while suffering for about 3 dB performance loss.

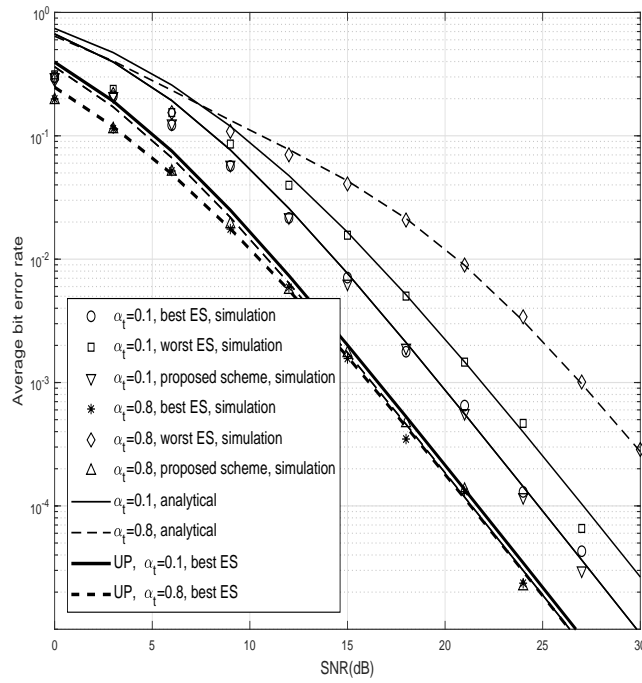


(a)

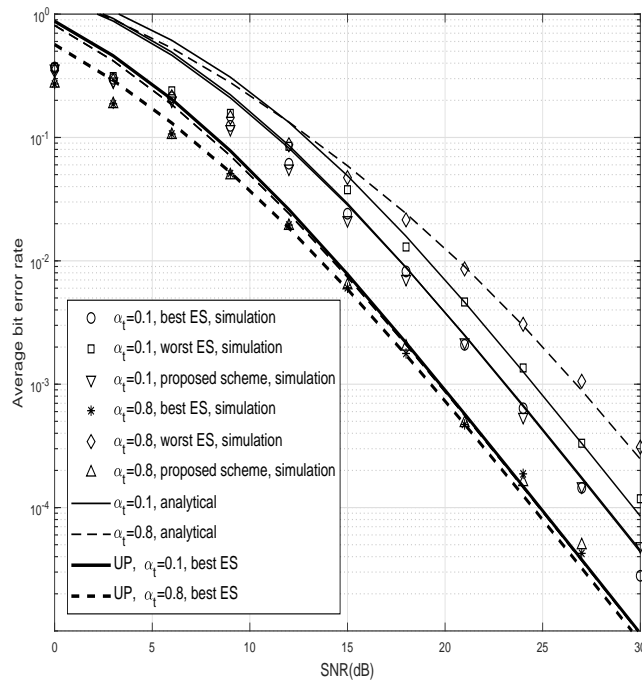


(b)

Figure 3.3: Performance comparison of the proposed algorithm with the optimum achievable ABEP and UP-GSM with different spatial correlation coefficients when $N_a = 2$, for a) $R = 3$ bpcu, b) $R = 4$ bpcu.



(a)



(b)

Figure 3.4: Performance comparison of the proposed algorithm with the optimum achievable ABEP and UP-GSM with different spatial correlation coefficients when $N_a = 3$, for a) $R = 3$ bpcu, b) $R = 4$ bpcu.

Chapter 4

Co-existence of LTE and Wi-Fi in Unlicensed Band

4.1 Introduction

The unprecedented data traffic, network densification, and massive connectivity (mostly due to new applications particularly Internet of things) are the key expectations of the next generation of wireless communication systems. With its advantages of unlicensed band operation, Wi-Fi has become a critical access technology for data offloading and massive connectivity. It is expected that Wi-Fi carries nearly half of the IP traffic through more than 540 million Wi-Fi hotspots by 2021 [31], which highlights the importance of Wi-Fi technology. However, there are several major challenges in the current Wi-Fi technology, which makes it difficult for service provisioning in more demanding industry applications. These challenges range from its contention-based protocol, which limits the achievable quality of service (QoS), to lack of inter-network coordination. Hence, to alleviate these challenges, utilizing unlicensed spectrum for LTE networks, which is recently proposed by Qualcomm [32], becomes a promising solution. However, the success of aforementioned spectrum shifting from licensed to unlicensed band for LTE protocol is conditioned on its highly efficient coexistence with densely deployed Wi-Fi networks which currently utilizes unlicensed spectrum.

To this end, different variations of this recently suggested shift can be classified to LTE unlicensed (LTE-U), LTE license-assessed access (LTE-LAA) and MuLTEfire, each of which

has its own characteristic. In other words, the main difference between these versions is the way they are adopted to fairly coexist with Wi-Fi networks.

The coexistence challenges mainly arise from the inherent difference between Wi-Fi and LTE protocols. To be more specific, schedule-based LTE protocol was originally meant to work in the licensed band and is designed for the continuous transmission. As opposed to LTE, Wi-Fi devices are contention-based and operate based on carrier sense multiple access with collision avoidance (CSMA/CA). In other words, Wi-Fi device senses the channel, if the channel is idle and remains idle for distributed inter-frame space (DIFS) amount of time, it starts the transmission. On the other hand, if the transmitter senses the channel as busy it generate the back-off time and start to count down the back-off time (it freezes the time if any other transmission occurs before the back-off time reaches to zero and resumes it once the other transmission finishes) and starts to transmit when the back-off time counts down to zero.

Considering the contrastive design approaches of Wi-Fi and LTE, it is very likely that Wi-Fi senses the channel busy and comes to silence when they work in the same band. In particular, one criterion to have an applicable LTE deployment in unlicensed band with the capability of simultaneously communications in existence of Wi-Fi networks is that the impact from LTE on a Wi-Fi AP should be less than that due to another Wi-Fi AP [33]. Nevertheless, there are several solutions to develop a fair coexistence mechanism. The first approach is to modify the current LTE-A protocol and utilize listen before talk (LBT) approach, which is analogous to CSMA/CA and is deployed in LTE-LAA. Notice that, LTE-LAA can achieve higher rate in comparison with the conventional LTE-A due to the data aggregation from both licensed and unlicensed bands.

Another promising solution to have effective coexistence of LTE in unlicensed spectrum and WiFi networks is that LTE-U controls its power in such a way that Wi-Fi senses the channel as vacant [34] while reducing the interference. The effect of interference due to the coexistence is studied in [35].

In summary, there is a lack of research considering the spatial domain as an additional degree of freedom to accommodate concurrent communications from different networks in unlicensed band. To address this problem, we exploit the concept of beamforming for LTE base station (BS). Notice that, beamforming is a well-studied technology, which steers the

beam to the desired direction and exploits the potential benefits of multiple-input multiple-output (MIMO) antenna, and in particular, space dimension to differentiate between different directions. While there are several works addressing the advantages of beamforming, it is not well-studied in the concept of coexistence of LTE and Wi-Fi. For this purpose, authors of [36] use the MUSIC algorithm, which uses the eigenspace of the noise and signal space, to obtain the direction of arrival (DoA) and utilize the null steering approach to mitigate the interference from LTE-LAA BS to Wi-Fi devices.

In this work, we focus on the coexistence of Wi-Fi and LTE-U through the exploration of beamforming in spatial domain. The proposed approach benefits from multiple antennas at the LTE-U base station that allows us exploit space dimension to mitigate the unwanted interference from LTE-U BS to the Wi-Fi APs. To obtain the beamforming vector of LTE-U, we study two separate constraint optimization problems. In the first approach, we aim to design the beamformer in such a way that the received power by Wi-Fi AP would be minimized while the received SNR by LTE-U user equipped (UE) satisfies a certain threshold. This minimized Wi-Fi received power helps it to identify the channel as vacant. In the second approach, we focus on maximizing the received SNR at UE subject to the maximum acceptable power threshold received by Wi-Fi AP.

This Chapter is organized as follows: Section II sheds light to the system model for coexistence of Wi-Fi and LTE-U. Consequently, two constraint optimization approaches, i.e., Wi-Fi received power minimization and UE received SNR maximization, are discussed in Section III and IV, respectively, followed by simulation results and conclusion in Section V and VI.

4.2 System Model

In this section, we establish the system model, where LTE-U small cell coexists with a Wi-Fi network and they share the same frequency band, i.e., 5 GHz. We suppose LTE-U and Wi-Fi AP are equipped with M and N antennas, respectively. We also assume the Wi-Fi access point (AP) aims to start the communication with Wi-Fi device while LTE-U is transmitting information to its cellular UE which has a single antenna. As mentioned earlier, if the received power experienced by Wi-Fi AP is more than a given threshold, it stops the Wi-Fi AP from the

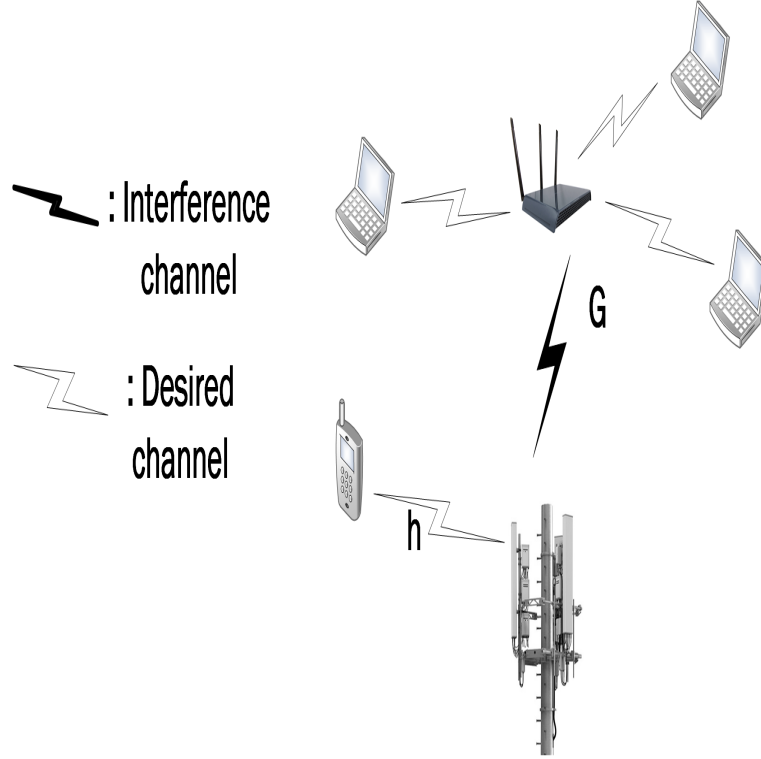


Figure 4.1: Networks coexistence and undesired interference from LTE-U on Wi-Fi.

transmission. To address this issue, we deploy beamforming at LTE-U BS to direct the beam to the desired direction such that the received power at Wi-Fi AP reduces while the SNR received by cellular UE increases. This transmission scenario is depicted in Fig. 4.1. Accordingly, the received signal at Wi-Fi AP and UE can be written as

$$\mathbf{y}_w = \sqrt{P}\mathbf{G}\mathbf{w}s + \mathbf{n}_w \quad (1)$$

and

$$y_u = \sqrt{P}\mathbf{h}^T\mathbf{w}s + n_u, \quad (2)$$

respectively, where \mathbf{y}_w and \mathbf{n}_w are $N \times 1$ vector, representing the received signal at Wi-Fi AP and noise vector whose elements follow from the zero-mean Gaussian random variable with variance σ_w^2 , i.e., $\mathbf{n}_w \sim \mathcal{CN}(0, \sigma_w^2\mathbf{I})$. \mathbf{G} denotes the $N \times M$ channel matrix between LTE-U BS and Wi-Fi AP. In addition, \mathbf{w} and s indicate the antenna weight vector and transmitted symbol

from LTE-U BS. We assume the transmitted signal is independent of channel realization and $E\{|s|^2\} = 1$, in which $E\{\cdot\}$ represents the expectation value and $|\cdot|$ is the norm of a complex number. P denotes the transmit power of LTE-U BS. Likewise, y_u and n_u are the received signal and noise at UE, where noise is zero-mean Gaussian random variable with variance σ_u^2 , i.e., $n_u \sim \mathcal{CN}(0, \sigma_u^2)$. \mathbf{h} is a $M \times 1$ channel vector between LTE-U BS and UE.

In the following, we evaluate two approaches to obtain antenna weight vector, \mathbf{w} . Namely, power minimization and SNR maximization.

4.3 Wi-Fi Received Power Minimization

In this part, our goal is to minimize the received power by Wi-Fi AP (P_w), while satisfying a given SNR for UE. This minimization problem can be formulated as

$$\begin{aligned} \min_{\mathbf{w}} \quad & P_w \\ \text{s.t.} \quad & \text{SNR} \geq \gamma \end{aligned} \quad (3)$$

where γ is a positive value and indicates the minimum acceptable SNR threshold at UE. In addition, received power at Wi-Fi AP can be expressed as

$$P_w = P\mathbf{w}^H \mathbf{G}' \mathbf{w} + N\sigma_w^2, \quad (4)$$

where $\mathbf{G}' = \mathbf{G}^H \mathbf{G}$ is the channel correlation matrix.

Notice that the last term in right side of equation (4), which represents the total noise power at Wi-Fi AP, is independent of antenna weight vector, \mathbf{w} , and thus can be eliminated in the minimization problem. Furthermore, considering (2), the received SNR at user end can be written as

$$\text{SNR} = \frac{P\mathbf{w}^H \mathbf{H}' \mathbf{w}}{\sigma_u^2}, \quad (5)$$

where \mathbf{H}' is defined as the correlation matrix given by $\mathbf{h}\mathbf{h}^H$. In particular, i th element of \mathbf{h} , i.e., h_i , represents the channel between i th antenna at LTE-U BS and UE. Accordingly, substituting

(4) and (5) in (3), the constraint optimization problem can be alternatively written as

$$\begin{aligned} \min_{\mathbf{w}} \quad & P\mathbf{w}^H\mathbf{G}'\mathbf{w} \\ \text{s.t.} \quad & \frac{P\mathbf{w}^H\mathbf{H}'\mathbf{w}}{\sigma_u^2} \geq \gamma. \end{aligned} \quad (6)$$

and can be further simplified to

$$\begin{aligned} \min_{\mathbf{w}} \quad & \mathbf{w}^H\mathbf{G}''\mathbf{w} \\ \text{s.t.} \quad & \mathbf{w}^H\mathbf{H}''\mathbf{w} \geq 1. \end{aligned} \quad (7)$$

in which we utilize the following equalities in the objective function and constraint, respectively.

$$\mathbf{G}'' = P\mathbf{G}', \quad (8)$$

$$\mathbf{H}'' = \frac{P}{\gamma\sigma_u^2}\mathbf{H}' \quad (9)$$

Also, notice that, \mathbf{G}'' and \mathbf{H}'' are both symmetric as they are the scaled version of the correlation matrices.

To have more insight on equation (7), we change the variable to $\tilde{\mathbf{w}} = \mathbf{H}''^{1/2}\mathbf{w}$, which makes us able to rewrite the optimization problem in form of

$$\begin{aligned} \min_{\tilde{\mathbf{w}}} \quad & \tilde{\mathbf{w}}^H\mathbf{Q}\tilde{\mathbf{w}} \\ \text{s.t.} \quad & \tilde{\mathbf{w}}^H\tilde{\mathbf{w}} = 1. \end{aligned} \quad (10)$$

where $\mathbf{Q} = \mathbf{H}''^{H^{-1/2}}\mathbf{G}''\mathbf{H}''^{-1/2}$. In addition, we replace the inequality in the constraint by equality. Notice that if the constraint is not active (i.e., inequality in constraint), the variable $\tilde{\mathbf{w}}$ can be scaled down to reach the equality, nevertheless it would result in a lower value of the objective function. In other words, optimum solution holds when the constraint is active.

In addition, the following proposition is deployed to achieve the analytical solution of our alternative optimization problem given by (10).

Proposition 4.3.1 *For any symmetric matrix \mathbf{A} , the optimum solution of problem*

$$\begin{aligned} \min_{\tilde{\mathbf{x}}} \quad & \tilde{\mathbf{x}}^H \mathbf{A} \tilde{\mathbf{x}} \\ \text{s.t.} \quad & \tilde{\mathbf{x}}^H \tilde{\mathbf{x}} = 1. \end{aligned} \quad (11)$$

is equal to the smallest eigenvalue of the matrix \mathbf{A} , i.e., $\lambda_{\min}(\mathbf{A})$.

Proof See Appendix A.

As stated in the proposition, the optimum antenna weight vector is the eigenvector of \mathbf{Q} corresponding to the smallest eigenvalue. Furthermore, setting $\tilde{\mathbf{w}}$ as the eigenvector which attributes to the smallest eigenvalue, the minimum solution of the problem in (10) is the minimum eigenvalue of matrix \mathbf{Q} , i.e., λ_{\min} .

4.4 UE Received SNR Maximization

Unlike in the last section, where we focused on minimizing the received power by Wi-Fi AP while satisfying quality of service (QoS) for LTE-U UE, in this part, our goal is to determine the antenna weight vector for LTE-U BS to maximize the SNR in UE subject to maximum acceptable power at Wi-Fi AP. Therefore, the problem can be formulated as

$$\begin{aligned} \max_{\mathbf{w}} \quad & \text{SNR} \\ \text{s.t.} \quad & P_w \leq P_{Th}. \end{aligned} \quad (12)$$

Substituting expressions for UE SNR and Wi-Fi received power as given by (4) and (5) in (12), we obtain

$$\begin{aligned} \max_{\mathbf{w}} \quad & \frac{P \mathbf{w}^H \mathbf{H}' \mathbf{w}}{\sigma_u^2} \\ \text{s.t.} \quad & P \mathbf{w}^H \mathbf{G}' \mathbf{w} + N \sigma_w^2 \leq P_{Th}. \end{aligned} \quad (13)$$

Considering the similar steps as given in Section III we can reformulate (13) as

$$\begin{aligned} \max_{\mathbf{w}} \quad & \mathbf{w}^H \mathbf{H}'' \mathbf{w} \\ \text{s.t.} \quad & \mathbf{w}^H \mathbf{G}'' \mathbf{w} = 1. \end{aligned} \quad (14)$$

where $\mathbf{H}''' = \frac{P}{\sigma_u^2} \mathbf{H}'$ and $\mathbf{G}''' = \frac{P}{P_{Th} - N\sigma_w^2} \mathbf{G}'$. Accordingly, the inequality constraint of (13) can be replaced by equality at the optimum point. Notice that if the constraint is inactive, one can scale up the antenna weight vector to reach the equality while increasing the objective function.

To solve (14) the modified version of (11) can be utilized where the minimization can be change to maximization which results to the optimum weight vector, i.e., the eigenvector $\mathbf{G}''' \mathbf{H}^{-1/2} \mathbf{H}''' \mathbf{G}'''^{-1/2}$ corresponding to the maximum eigenvalue. In addition, the maximum solution can be achieved to be the maximum eigenvalue of $\mathbf{G}''' \mathbf{H}^{-1/2} \mathbf{H}''' \mathbf{G}'''^{-1/2}$.

4.5 Simulation Results

In this section, we present the simulation results. We assume number of antennas at LTE-U BS and Wi-Fi AP to be 8, i.e., $M = N = 8$, which is compatible with LTE-A standard [37] and 802.11 ac [38]. We assume that the channel realizations from LTE-U BS to UE (i.e., h_i for $i \in \{1, 2, \dots, M\}$) are independent of those from LTE-U BS to Wi-Fi AP (i.e., $g_{p,q}$ for $p \in \{1, 2, \dots, N\}$ and $q \in \{1, 2, \dots, M\}$). As in [39], we assume that each channel element composed of a fixed and variable component, which can be represented as

$$h_i = \bar{h}_i + \tilde{h}_i \quad (15)$$

where \bar{h}_i denotes the fixed part of the channel and \tilde{h}_i represents a zero-mean random variable. We also assume that \tilde{h}_i is independent of $\tilde{h}_{i'}$, for $i \neq i'$. Therefore, expected value of h_i can written as

$$\bar{h}_i = \frac{e^{j\theta_i}}{\sqrt{1 + \alpha_h}}. \quad (16)$$

where θ_i is a random variable which is uniformly distributed between 0 and 2π , i.e., $\theta_i \sim U[0, 2\pi]$,

We also assume, without loss of generality, that the variance of h_i follows the following

expression

$$\text{var}(h_i) = \text{var}(\tilde{h}_i) = \frac{\alpha_h}{1 + \alpha_h}. \quad (17)$$

where α_h in (16) and (17) represents the amount of uncertainty we have for channel realization.

Hence, elements of the matrix \mathbf{H}' can be represented as

$$h'_{i,j} = \begin{cases} \bar{h}_{i,j}\bar{h}_{i,j}^* + \frac{\alpha_h}{1+\alpha_h} & \text{if } i = j \\ \bar{h}_{i,j}\bar{h}_{i,j}^* & \text{elseif } i \neq j \end{cases} \quad (18)$$

where $(.)^*$ denotes the conjugate of a variable and $i, j \in \{1, 2, \dots, M\}$.

The elements of channel matrix from LTE-U BS to Wi-Fi AP ($g_{p,q}$) can be modeled in a similar way as a combination of a fixed and variable part given by

$$g_{p,q} = \bar{g}_{p,q} + \tilde{g}_{p,q} \quad (19)$$

in which

$$\bar{g}_{p,q} = \frac{e^{j\phi_{p,q}}}{\sqrt{1 + \alpha_g}} \quad (20)$$

is the mean and fixed part of the channel and $\phi_{p,q}$ is a uniformly distributed random variable in the interval 0 and 2π , i.e., $\phi_{p,q} \sim U[0, 2\pi]$. In addition, the variance of the variable component can be written as

$$\text{var}(g_{p,q}) = \text{var}(\tilde{g}_{p,q}) = \frac{\alpha_g}{1 + \alpha_g}. \quad (21)$$

As for the elements of \mathbf{h} , we assume $\tilde{g}_{p,q}$ is independent of $\tilde{g}_{p',q'}$ for all $p \neq p'$ and $q \neq q'$.

Likewise, elements of the matrix \mathbf{G}' can be written as

$$g'_{p,q} = \begin{cases} \bar{g}_{p,q}\bar{g}_{p,q}^* + \frac{\alpha_g}{1+\alpha_g} & \text{if } p = q \\ \bar{g}_{p,q}\bar{g}_{p,q}^* & \text{elseif } p \neq q \end{cases} \quad (22)$$

for $p, q \in \{1, 2, \dots, M\}$.

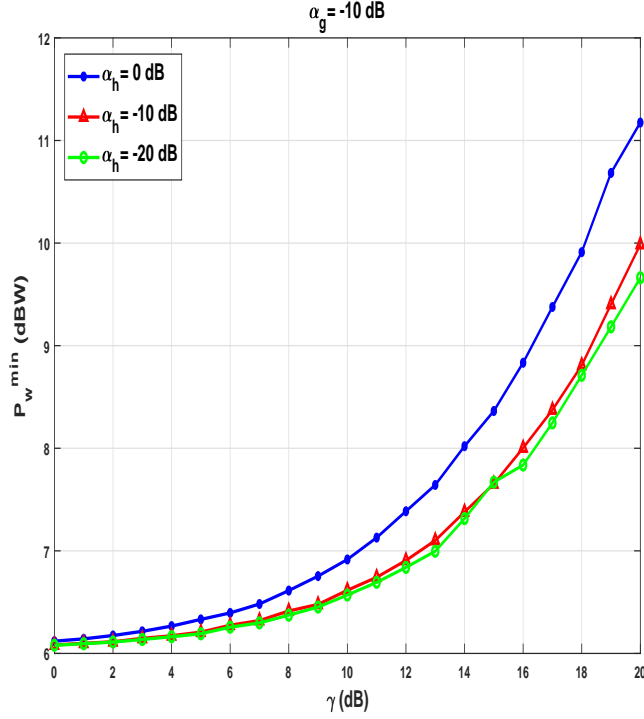


Figure 4.2: Minimum received power by Wi-Fi AP vs. QoS threshold for UE, $\alpha_g = -10$ dB and $\alpha_h = \{-20, -10, 0\}$.

Fig. 4.2 depicts the received power by Wi-Fi AP while the transmitted power of LTE-U BS is set to 1.5 Watt. In addition, we assume that the variance of noise is 0.5, i.e., $\sigma_u^2 = \sigma_w^2 = 0.5$. We also assume that uncertainty of channel realization from LTE-U BS and Wi-Fi AP is fixed and set to -10 dB, i.e., $\alpha_g = -10$ dB. It can be seen from the Figure that increasing the QoS threshold at UE increases the received signal at Wi-Fi AP. Furthermore, increasing the uncertainty of the channel realizations leads to higher received power by Wi-Fi AP. However, as in [36] and [40], assuming 10 dBW as the power limit, beyond which Wi-Fi AP sense the channel as busy and keep silent, we can guarantee the QoS (i.e., SNR) of 18, 20, and 20 dB for channel uncertainty of 0, -10 , and -20 , respectively.

Fig. 4.3 illustrate the minimized power obtained at Wi-Fi AP when $\alpha_h = -10$ dB and for different values of α_g , i.e., $\alpha_g = \{0, -10, -20\}$ dB. Rest of the parameters remain the same as those of Fig. 4.2. While the general trend is the same as in Fig. 4.2, Wi-Fi received power shows more sensitive behaviour with respect to the uncertainty of the channel connecting LTE-U BS and Wi-Fi AP. Specifically, there is more change of received power for a given change

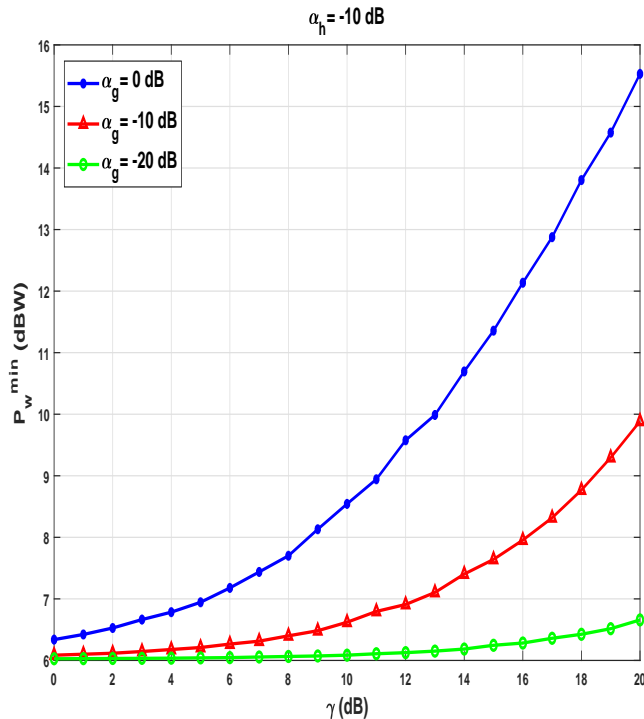


Figure 4.3: Minimum received power by Wi-Fi AP vs. QoS threshold for UE, $\alpha_h = -10$ dB and $\alpha_g = \{-20, -10, 0\}$.

in uncertainty in comparison with Fig. 4.2. Fig. 4.3 also shows that UE can achieve maximum SNR of 13 dB when $\alpha_g = 0$ dB. In other words, Wi-Fi AP can feel the channel as vacant while we can increase the QoS of UE up to 13 dB. For higher channel certainty (lower α_g), SNR can be increased up to 20 dB and even higher.

Fig. 4.4 illustrates the results of second optimization problem, i.e., SNR maximization at UE subject to power constraint at Wi-Fi AP for $\alpha_g = -10$ dB while uncertainty of channel \mathbf{h} changes among -20 , -10 , and 0 dB. It shows that even for high uncertainty, i.e., $\alpha_h = 0$ dB, UE can achieve up to around 22 dB SNR. It can be also seen that even for a small value of Wi-Fi power threshold, the SNR of more than 17 dB is feasible.

Fig. 4.5 shows the amount of maximum received SNR at UE terminal versus different values of power threshold at Wi-Fi AP. The results are shown for the same set of parameter as those in Fig. 4.4 and fixed value for α_h while varying the amount of α_g . The Figure shows that even for high level of uncertainty, UE can achieve satisfactory amount of SNR. This QoS substantially increase as a result of reduced channel uncertainty.

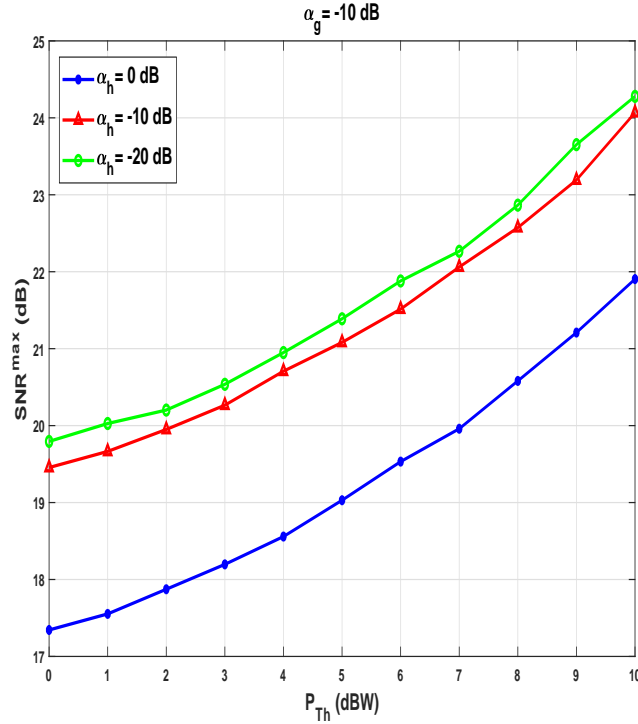


Figure 4.4: Maximum received SNR by UE vs. power threshold for Wi-Fi AP, $\alpha_g = -10$ dB and $\alpha_h = \{-20, -10, 0\}$.

4.6 Conclusion

In this work, we consider the coexistence of LTE-U and Wi-Fi networks. We deploy beamforming technique at LTE-U BS such that Wi-Fi AP sense the channel as unoccupied, which offers a fair coexistence by making Wi-Fi AP capable of starting the transmission in presence of LTE-U network. We develop two optimization problems which results in a closed form solution to calculate the antenna weight vector at LTE-U BS in such a way that the two networks meet the coexistence requirement. In particular, first, we consider minimizing the received power at Wi-Fi AP while satisfying the QoS constraint at LTE-U UE. Secondly, we maximized the SNR at LTE-U UE in such a way that received power at Wi-Fi AP remains below a certain threshold. Finally, simulation results confirm the benefit of beamforming as an effective coexisting mechanism between Wi-Fi and LTE-U.

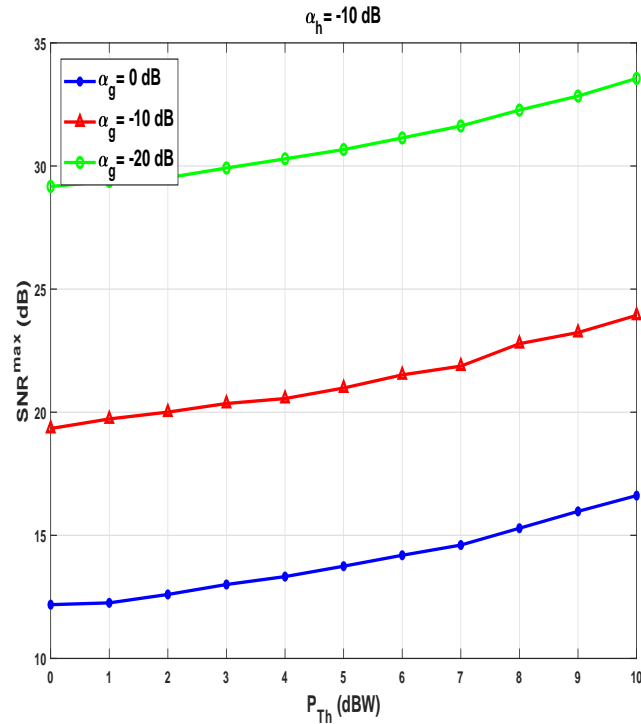


Figure 4.5: Maximum received SNR by UE vs. power threshold for Wi-Fi AP, $\alpha_h = -10$ dB and $\alpha_g = \{-20, -10, 0\}$.

4.7 Proof of Proposition 4.3.1

We use the fact that any $n \times n$ symmetric matrix \mathbf{A} can be decomposed and written in terms of its eigenvalues and eigenvectors as $\mathbf{A} = \mathbf{U}^H \mathbf{\Lambda} \mathbf{U}$, where $\mathbf{\Lambda}$ is a diagonalized matrix whose diagonal elements indicate the eigenvalue of matrix \mathbf{A} and \mathbf{U} is a unitary matrix. Hence, the optimization problem given by (11) can be expressed as

$$\begin{aligned} \min_{\tilde{\mathbf{x}}} \quad & \tilde{\mathbf{x}}^H \mathbf{U}^H \mathbf{\Lambda} \mathbf{U} \tilde{\mathbf{x}} \\ \text{s.t.} \quad & \tilde{\mathbf{x}}^H \tilde{\mathbf{x}} = 1. \end{aligned} \quad (23)$$

Changing the variable $\mathbf{z} = \mathbf{U} \tilde{\mathbf{x}}$ results in

$$\begin{aligned} \min_{\mathbf{z}} \quad & \sum_{p=1}^n \lambda_p z_p^2 \\ \text{s.t.} \quad & \sum_{p=1}^n z_p^2 = 1, \end{aligned} \quad (24)$$

where λ_p s for $p \in \{1, 2, \dots, n\}$ are the eigenvalues of matrix \mathbf{A} . Notice that, as the matrix \mathbf{U} is a unitary matrix, it can be concluded that $\mathbf{z}^H \mathbf{z} = 1$, which is further simplified to the constraint in (24). Notice that if λ_{j^*} is the smallest eigenvalue then the optimum solution would be the unit vector whose all elements are zero except the j^* th element which is equal to 1, i.e., $z_p = 1$ if $p = j^*$ and $z_p = 0$ for $p \neq j^*$. Therefore the optimum solution is λ_{j^*} .

Chapter 5

NOMA-based Communication with Spatial Modulation

5.1 Introduction

As mentioned earlier, ever increasing demand for connectivity and densification highlights the importance of more efficient system design in order to further increase the capacity and throughput of communication systems. Unlike the conventional approaches for multiple access scenarios, such as time division multiple access (TDMA), and frequency division multiple access (FDMA), where orthogonal resources (time and frequency) are allocated to different users, non-orthogonal multiple access aims to assign the same time and frequency slots to users and differentiate them in a non-orthogonal manner [5], and thus achieves the spectrum efficient multiple access. For dense environments, NOMA is more beneficial as it can support more users with same resource blocks (frequency and time). In addition, NOMA may provide service to users who have not been served for a long period of time (because of poor channel conditions) while offering transmission to users with rich channel realization. Doing so, the fairness is improved in comparison with orthogonal multiple access (OMA) [41]. Notice that there are different types of non-orthogonal multiple access which can be divided into three main categories based on power, code, and pattern [42], among which power domain NOMA has become more attractive.

In pattern division multiple access (PDMA) [42], each user's data is mapped to a group of

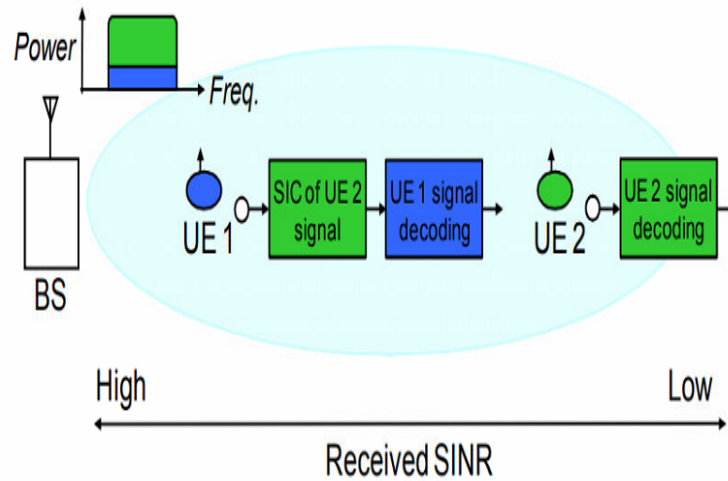


Figure 5.1: Principal of NOMA communication with SIC detection [5].

resources. In this concept, resource may refer to either time, frequency, space or any combination of those. To accomplish the non-orthogonality in power domain, various amounts of powers are allocated to different users with different channel gains. In addition, users deploy successive interference cancellation (which has been discussed in Chapter 2) for the purpose of detection. For the sake of illustration, the power-based NOMA (which has been considered through this chapter) with SIC detection algorithm has been depicted in Fig. 5.1.

Motivated by the fact that user end devices are small and power limited, it is critical to design a transmission scheme that meets these constraints. As such, we investigate on the combination of SM and NOMA, which can benefit from advantages of NOMA while offering power efficient transmission with limited number of RF chains. In this Chapter, first we calculate the probability of error for users with SM-NOMA. Later on, we focus on the achievable rate and capacity calculation to evaluate the effect of user pairing based on different user distances from BS. In capacity calculation, we start with normal multi-user SISO communication and investigate on the effect of Rician factor. After that we move to MIMO transmission scenario and implement SM-NOMA.

5.2 System Model

We consider an uplink transmission system with two users as in [43]. Notice that larger number of users can be divided into groups of two users and different groups can access the resources in an orthogonal manner. Furthermore, we assume there are N_t antenna elements at user terminal (we assume the same number of antennas for all users, without loss of generality) and N_r antennas at the BS. At each transmission instance, the input bits of each user is divided into two sub-streams which are used to select one activated antennas and one constellation symbol to be transmitted via selected antenna. To be more specific, assume ℓ_n and m_n bits of the first and second sub-streams of the n -th user ($n \in \{1, 2\}$) are mapped to the antenna set and constellation space of size $L = 2^{\ell_n}$ and $M = 2^{m_n}$, respectively. Assume v -th symbol is transmitted by u -th antenna, where $v \in \{1, \dots, M\}$ and $u \in \{1, \dots, L\}$. In particular, transmitted signal of the n -th user can be shown as

$$\mathbf{x}_n = s_{n,v} \mathbf{e}_u, \quad (1)$$

in which \mathbf{e}_u is the u -th column of identity matrix. We deploy non-orthogonal multiple access, where power domain is utilized to differentiate users. As such, users are first ordered by their channel gains. In order to have the fair quality of service (QoS), user with lower channel gain (user which is far from the transmitter) transmits its signal with higher power. Accordingly, signal of the user with high channel gain (close to the transmitter) is transmitted with lower power. Therefore, the overall received signal at BS is a combination of the signal from both users, shown by

$$\mathbf{y} = \sqrt{P_1} \mathbf{H}_1 \mathbf{x}_1 + \sqrt{P_2} \mathbf{H}_2 \mathbf{x}_2 + \boldsymbol{\nu} \quad (2)$$

where P_n denotes the power assigned to n -th user. Without loss of generality, we assume $P_1 > P_2$. We also assume normalized total power and thus, $\sum_{n=1}^2 P_n = 1$.

The transmitted signal from n -th user, \mathbf{x}_n , is transmitted through $N_r \times N_t$ channel. Assume that the channel between transmitter and user n is modeled as a flat fading channel and consists

of a fixed and variable part given by

$$\mathbf{H}_n = \sqrt{\frac{K}{1+K}} \bar{\mathbf{H}}_n + \sqrt{\frac{1}{1+K}} \tilde{\mathbf{H}}_n \quad (3)$$

where $\bar{\mathbf{H}}_n$ is the deterministic part of the channel representing the line of sight (LOS) component. $\tilde{\mathbf{H}}_n$ denotes multipath fading which is modeled as Rayleigh fading channel. K is the ratio of the LOS component to NLOS components and is known as Rician factor.

At BS, the signal from user with higher power is interpreted as interference while the signal of other user with lower power is considered as noise. Therefore, SIC (which has been described in Chapter 2) algorithm can be implemented. More specifically, BS detects the signal from the first user, subtracts it from the overall received signal, and then decodes the signal from the second user.

Notice that the received signal at BS after interference cancellation is given by

$$\tilde{\mathbf{y}} = \mathbf{y} - \sqrt{p_1} \mathbf{H}_1 \hat{\mathbf{x}}_1. \quad (4)$$

5.3 Average Bit Error Rate Analysis

As mentioned earlier, SIC detection can be used at BS to detect second user's data and to cancel the interference from high-power signal from first user. Notice that, for general case of $n > 2$ users, we can deploy ML for n -th user to jointly detect the symbol and activated antennas of user j , for $j \in \{1, \dots, n\}$, from which $n - 1$ detection is done for the purpose of interference cancellation which are done in the order of power reduction, and the last detection is done to detect the data from n -th user. Nevertheless, in this part, we assume two users. Therefore, to detect to first user's signal, BS considers the second user's signal as part of the noise. Thus, considering (2) for the first user signal detection, we have

$$\begin{aligned} \mathbf{y} &= \sqrt{P_1} \mathbf{H}_1 \mathbf{x}_1 + \sqrt{P_2} \mathbf{H}_2 \mathbf{x}_2 + \nu \\ &= \sqrt{P_1} \mathbf{H}_1 \mathbf{x}_1 + \nu' \end{aligned} \quad (5)$$

where $\boldsymbol{\nu}' = \sqrt{P_2}\mathbf{H}_2\mathbf{x}_2 + \boldsymbol{\nu}$ is a zero-mean complex Gaussian random variable with variance $(\sigma^2 + P_2 | \mathbf{H}_2\mathbf{x}_2|^2)\mathbf{I}$, i.e., $\sim (0, (\sigma^2 + P_2 | \mathbf{H}_2\mathbf{x}_2|^2)\mathbf{I})$. Therefore, BS deploys ML to detect \mathbf{x}_1 by minimizing the distance metric as follows

$$(\hat{v}_1, \hat{u}_1) = \min D(\mathbf{y} - \sqrt{P_1}\mathbf{H}_1\mathbf{x}_1). \quad (6)$$

Notice that, calculating the signal from first user, signal of user 2 is consider as part of the noise, $\boldsymbol{\nu}'$. Thus, pairwise error probability can be written as

$$P\{\text{noise} > d/2\}. \quad (7)$$

Note that noise follows a Gaussian mixture distribution and therefore (7) can be written as given in [44] by

$$\begin{aligned} & P\{\text{noise} > d/2\} \\ &= \int_{-\frac{d}{2}}^{\infty} \left(\frac{1}{\sqrt{\pi\sigma^2}} \exp\left(-\frac{\alpha}{\sigma^2}\right) + \frac{1}{\sqrt{\pi\rho_2}} \exp\left(-\frac{\alpha}{\rho_2}\right) \right) d\alpha \\ &= \int_{-\frac{d}{2}}^{\infty} \frac{1}{\sqrt{\pi\sigma^2}} \exp\left(-\frac{\alpha}{\sigma^2}\right) d\alpha + \int_{-\frac{d}{2}}^{\infty} \frac{1}{\sqrt{\pi\rho_2}} \exp\left(-\frac{\alpha}{\rho_2}\right) d\alpha \end{aligned} \quad (8)$$

Changing the variable in first and second term of right hand side of (8) as $\lambda_1 = \alpha \sqrt{\frac{2}{\sigma^2}}$ and $\lambda_2 = \alpha \sqrt{\frac{2}{\rho_2}}$, respectively, results in

$$P\{\text{noise} > d/2\} = Q\left(\sqrt{\frac{\|\mathbf{d}\|^2}{2N_0}}\right) + Q\left(\sqrt{\frac{\|\mathbf{d}\|^2}{2\rho_2}}\right) \quad (9)$$

where \mathbf{d} is defined as $\mathbf{d} = \mathbf{H}\mathbf{x}_1 - \mathbf{H}\hat{\mathbf{x}}_1$ and can be alternatively written as $\mathbf{d} = (\mathbf{Y} \otimes \mathbf{I}) \text{vec}(\mathbf{H})$, in which $\mathbf{Y} = (\mathbf{x}_1 - \hat{\mathbf{x}}_1)^T$. Similar to [45], we can show that \mathbf{d} is a proper complex Gaussian

(PCG) random variable whose mean and variance are derived as

$$\mathbf{m}_d = \sqrt{\frac{K}{1+K}} (\Upsilon \otimes \mathbf{I}) \text{vec}(\tilde{\mathbf{H}}) \quad (10)$$

$$\Gamma_d = \frac{1}{1+K} (\Upsilon \otimes \mathbf{I}) \Psi (\Upsilon \otimes \mathbf{I})^\dagger. \quad (11)$$

Consequently, estimating the signal from the first user, and after SIC, data from user 2 can be estimated by

$$(\hat{v}_2, \hat{u}_2) = \min D(\tilde{\mathbf{y}} - \sqrt{P_2} \mathbf{H}_2 \mathbf{x}_2). \quad (12)$$

5.3.1 Simulation Results

In this section, we evaluate the performance of signal detection from both users in terms of their average bit error rate based on the derived equations and compare them with Monte Carlo simulations. In all curves, the theoretical results related to first and second users are shown by solid line and dashed line, respectively, while the Monte Carlo simulations are shown by markers.

In order to split the total power, we assume the same received SINR for both users at BS. In particular, assume that first user is located in more distance from BS compare to the second user, i.e., the channel of first user is poor while second user has high channel gain. Therefore, the assumption of equal received SINR can be written as

$$\frac{P_1}{P_2 + \sigma^2} = \frac{P_2}{\sigma^2}. \quad (13)$$

In addition, power of two users need to satisfy the overall power condition given by

$$P_1 + P_2 = P, \quad (14)$$

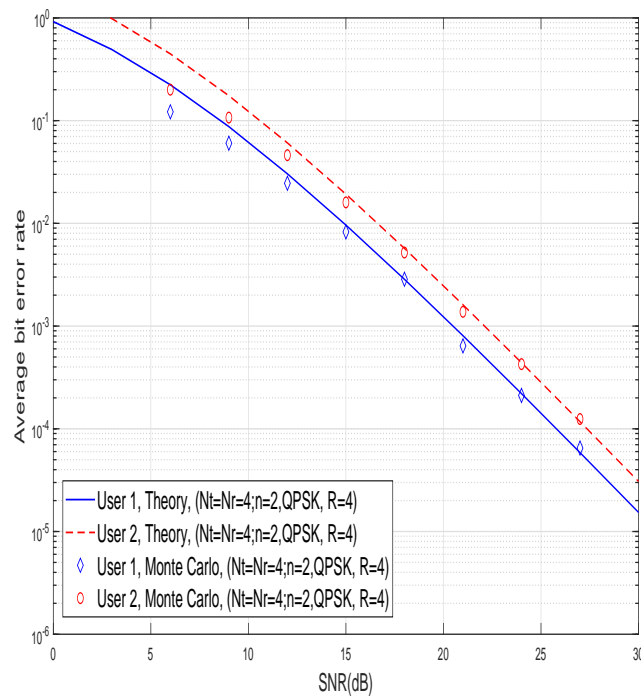


Figure 5.2: Performance analysis of two users with NOMA transmission and same spectral efficiencies, i.e., $R = 4$.

where P is the overall available power. Notice that equations (13) and (14) can be written as

$$\left(P_2 + \sigma^2\right)^2 = \sigma^2 P + \sigma^4, \quad (15)$$

which can be simplified to $P_2 = \sqrt{\sigma^2 P + \sigma^4} - \sigma^2$ and $P_1 = P - P_2 = 1 - P_2$.

In Fig. 5.2, we assume the same number of antennas for the first and second user, with spectral efficiency of 4.

Fig. 5.3 depicts the more general scenario, in which number of antennas and spectral efficiencies vary for different users. In particular, we assume 2 bpcu for the first user with two transmit antennas and 4 bpcu for the second user which transmits from four antenna elements. In all curves, the simulation results are all tightly match with the theoretical derivations. It can be seen from the Figures that performance of first user is better than that of second user. This observation can be justified by the fact that erroneous detection of signal from first user is propagated through the SIC detection.

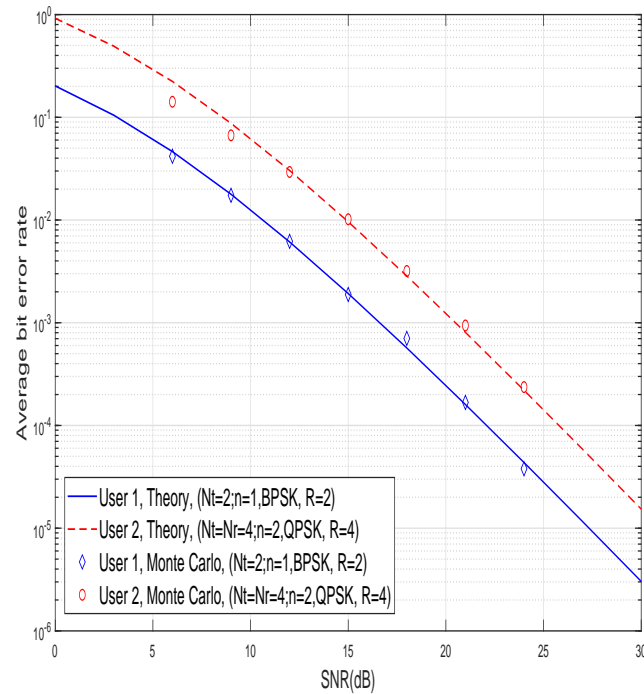


Figure 5.3: Performance analysis of two users with NOMA transmission and different spectral efficiencies and different number of antennas.

5.4 User Pairing with Fixed Power Allocation

In this Section, we consider user pairing in NOMA transmission scheme. Notice that, two different power allocations, namely fixed power allocation and cognitive radio approach of power allocation, has been proposed in [46]. It has been shown that in fixed power allocation, the NOMA outperforms the OMA communication when the users experience different channels and as this difference increases it enlarges the gap between performance of NOMA and OMA. Nevertheless, unlike fixed power allocation, in cognitive approach, the advantage of NOMA is highlighted as the difference between the channels seen by two users becomes smaller. Through this thesis, our focus is on fixed power allocation.

In the following, we start with the SISO transmission as in [46] to evaluate the effect of pairing in NOMA and compare it with OMA performance. Later on, we extend the results to more general channel models (Rician channel) and assess the impact of different Rician factors.

5.4.1 User pairing in SISO NOMA

Consider transmission system, where a single antenna BS serves M single antenna users under the same available resources, i.e., time and frequency. To start with and without loss of generality, assume h_i represents the channel coefficient from i -th single antenna user to the BS such that

$$|h_1|^2 \leq \dots \leq |h_M|^2. \quad (16)$$

In addition, assume the fixed and normalized power allocation for n -th and m -th user, i.e., a_n and a_m , such that $a_n^2 + a_m^2 = 1$. Now, the question is how to select two users so that the system achieves higher performance in term of sum rate capacity. Based on the principal of NOMA and considering (16), assuming $m < n$ implies that $|h_m|^2 \leq |h_n|^2$ and thus $a_m \geq a_n$. Therefore, achievable rates of m -th and n -th user can be respectively written as

$$R_m = \log \left(1 + \frac{|h_m|^2 a_m^2}{|h_m|^2 a_n^2 + \frac{1}{\rho}} \right), \quad (17)$$

and

$$R_n = \log \left(1 + \rho |h_n|^2 a_n^2 \right). \quad (18)$$

Before further investigation and for the sake of illustration, assume ten sorted users (based on their channel) out of which we select two users, pair them in a group, and compare the performance of NOMA and OMA transmission. Fig. 5.4 represents the capacity of NOMA and compare it with its OMA correspondence for different user orders. We assume 1/5 and 4/5 of total power is assigned to data transmission from the first and second users, respectively.

In this Figure, the performances of NOMA are shown with solid lines while those of OMA are depicted by dashed lines. In addition, different colors represent pairing with different orders. In particular, pairing users with best and worst channels are shown by color red while the sum rate capacity achieved from the scenario, where the user with worst channel is paired with the user that experiences the medium channel condition, is depicted by color blue. It can

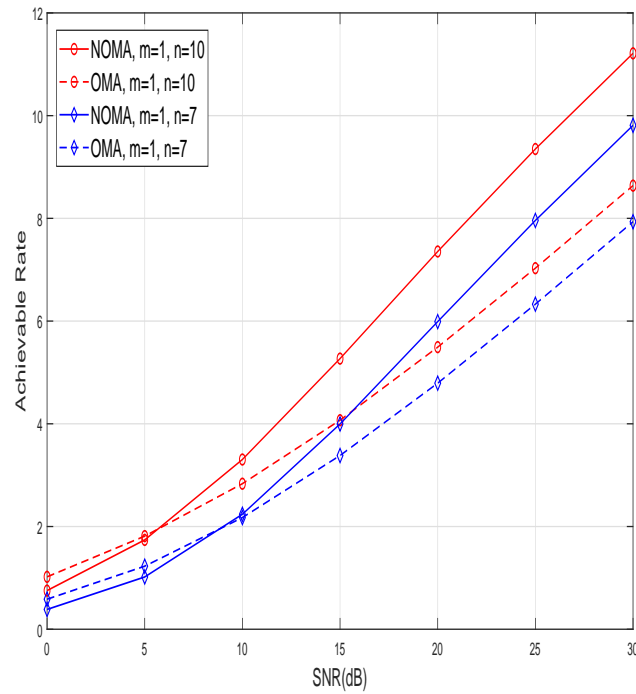


Figure 5.4: Capacity comparison of NOMA and OMA, SISO, $a_n^2 = 1/5$ and $a_m^2 = 4/5$, $K = 0$.

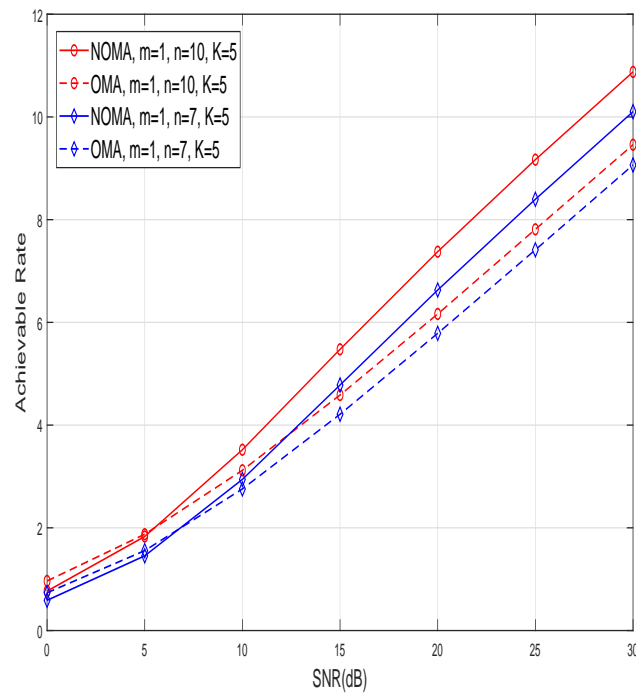


Figure 5.5: Capacity comparison of NOMA and OMA, SISO, $a_n^2 = 1/5$ and $a_m^2 = 4/5$, $K = 5$.

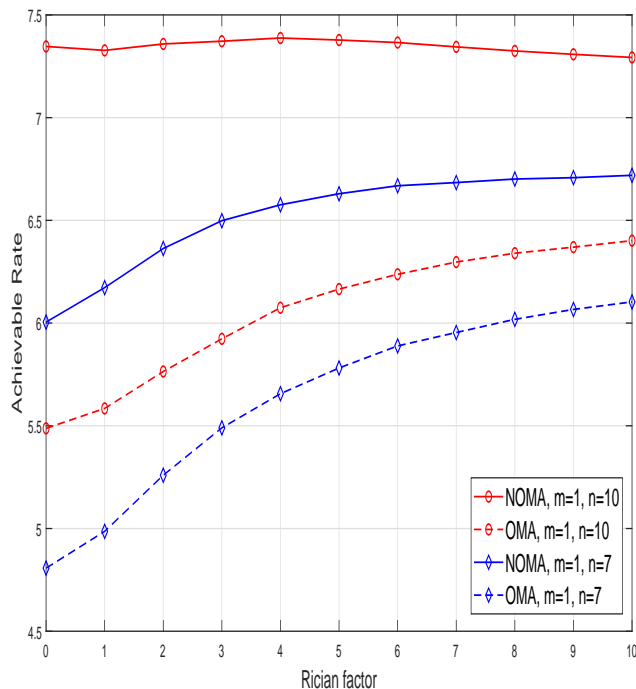


Figure 5.6: Capacity comparison of NOMA and OMA, SISO, $a_n^2 = 1/5$ and $a_m^2 = 4/5$, $SNR = 20$ dB.

be seen that more channel differentiation enhances the performance of the system. In addition, the advantages of NOMA over OMA can be seen from the Figure.

Fig. 5.5 depicts similar scenario under Rician channel model. In this Figure, Rician factor is set to be 5, i.e., $K = 5$ and the same observations can be made as those for Rayleigh channel.

In Fig. 5.6, we set the SNR to be fixed and equal to 20 dB and plot the achievable rate versus different values of Rician factors. The first observation is that for all cases with same pairs of users, NOMA outperforms OMA. In addition, it can be seen that the performance of OMA is more sensitive to the Rician factor compared with its NOMA correspondence.

An alternative approach that sheds light on the performance of NOMA and enables us to consider user pairing strategy is to evaluate the sum rate capacity and investigate the probability that OMA systems outperform NOMA. Such a criteria has been described in [46] and shown by:

$$\Pr(R_m + R_n < R_m^O + R_n^O), \quad (19)$$

where R_i^O represents the achievable rate of i -th user (for $i \in \{m, n\}$) in OMA and can be calculated as

$$R_i^O = \frac{1}{2} \log \left(1 + \rho |h_i|^2 \right). \quad (20)$$

Notice that in OMA there is no interference, and ρ denotes the SNR for both users. Nevertheless, the coefficient $1/2$ shows that each user uses only half of the resources (such as bandwidth). Considering (17)-(18) and (20), sum rate of NOMA and OMA can be evaluated as

$$R_m + R_n = \log \left(\left(1 + \frac{|h_m|^2 a_m^2}{|h_m|^2 a_n^2 + \frac{1}{\rho}} \right) \left(1 + \rho |h_n|^2 a_n^2 \right) \right) \quad (21)$$

and

$$R_m^O + R_n^O = \log \left(\left(1 + \rho |h_m|^2 \right)^{\frac{1}{2}} \left(1 + \rho |h_n|^2 \right)^{\frac{1}{2}} \right), \quad (22)$$

respectively. Therefore, replacing (21) and (22) in (19) results in

$$\begin{aligned} & \Pr \left(R_m + R_n < R_m^O + R_n^O \right) \\ = & \Pr \left(\log \left(\left(1 + \frac{|h_m|^2 a_m^2}{|h_m|^2 a_n^2 + \frac{1}{\rho}} \right) \left(1 + \rho |h_n|^2 a_n^2 \right) \right) < \log \left(\left(1 + \rho |h_m|^2 \right)^{\frac{1}{2}} \left(1 + \rho |h_n|^2 \right)^{\frac{1}{2}} \right) \right). \end{aligned} \quad (23)$$

Notice that, since the logarithm function is a monotonically increasing function, (23) can be simplified to

$$\begin{aligned} & \Pr \left(R_m + R_n < R_m^O + R_n^O \right) \\ = & \Pr \left(\left(1 + \frac{|h_m|^2 a_m^2}{|h_m|^2 a_n^2 + \frac{1}{\rho}} \right) \left(1 + \rho |h_n|^2 a_n^2 \right) < \left(1 + \rho |h_m|^2 \right)^{\frac{1}{2}} \left(1 + \rho |h_n|^2 \right)^{\frac{1}{2}} \right) \end{aligned} \quad (24)$$

which can be further written as:

$$\begin{aligned}
& \Pr(R_m + R_n < R_m^O + R_n^O) \\
&= \Pr\left(\left(\frac{\rho|h_m|^2 a_n^2 + 1 + \rho|h_m|^2 a_m^2}{\rho|h_m|^2 a_n^2 + 1}\right)^2 (1 + \rho|h_n|^2 a_n^2)^2 < (1 + \rho|h_m|^2)(1 + \rho|h_n|^2)\right) \\
&= \Pr\left(\left(\frac{1 + \rho|h_m|^2}{1 + \rho|h_m|^2 a_n^2}\right)^2 (1 + \rho|h_n|^2 a_n^2)^2 < (1 + \rho|h_m|^2)(1 + \rho|h_n|^2)\right) \\
&= \Pr\left(\frac{1 + \rho|h_m|^2}{(1 + \rho|h_m|^2 a_n^2)^2} < \frac{1 + \rho|h_n|^2}{(1 + \rho|h_n|^2 a_n^2)^2}\right). \tag{25}
\end{aligned}$$

Now, for the sake of simplicity, we change the variables such that $w = \rho|h_m|^2$ and $z = \rho|h_n|^2$. Notice that considering (16), variables w and z are ordered random variables. Before further evaluations, let us illustrate some of the properties of ordered random variables [47]. For this reason, assume that $X_{(i)}$ shows ordered random variable, such that $X_{(1)} \leq X_{(2)} \leq \dots \leq X_{(L)}$ whereas X_i represents un-ordered random variable. For the sake of clarification, consider the following example

Example Assume that a series of random variables are consequentially generated having the following realization:

$$X_1 = 5, \quad X_2 = 1, \quad X_3 = 4, \quad X_4 = 10. \tag{26}$$

The above random variables are known to be un-ordered. Nevertheless, the ordered version of such random variables can be written as

$$X_{(1)} = 1, \quad X_{(2)} = 4, \quad X_{(3)} = 5, \quad X_{(4)} = 10. \tag{27}$$

In light of the ordered random variables as mentioned above, cumulative distribution function

(CDF) of r -th ordered random variable, i.e., F_r can be formulated as

$$\begin{aligned}
 F_r(x) &= \Pr(X_{(r)} \leq x) \\
 &= \Pr(\text{at least } r \text{ random variables} \leq x) \\
 &= \sum_{i=r}^L \binom{L}{i} P^i(x) (1 - P(x))^{L-i}
 \end{aligned} \tag{28}$$

where $P(x)$ denotes the CDF of an un-ordered random variable and

$$\binom{L}{i} = \frac{L!}{i!(L-i)!} \tag{29}$$

shows binomial coefficient. In addition, probability density function (PDF) of an ordered random variable, $X_{(r)}$ can be calculated as in [47] given by

$$\begin{aligned}
 f_r(x) &= \Pr((r-1) \text{ random variables} < x, r\text{-th random variable} = x, \\
 &\quad (L-r) \text{ random variables} > x)
 \end{aligned} \tag{30}$$

which can be mathematically written as

$$f_r(x) = \binom{L}{r-1} \binom{L-r+1}{1} P^{r-1}(x) p(x) (1 - P(x))^{L-r}. \tag{31}$$

Now, consider two ordered random variable, i.e., $X_{(r)}$ and $X_{(s)}$, where $r < s$. The joint PDF of these two random variables, i.e., $f_{r,s}(x, y)$ can be expressed as

$$\begin{aligned}
 f_{r,s}(x, y) &= \Pr(X_{(r)} = x, X_{(s)} = y) \\
 &= \Pr((r-1) \text{ random variables} < x, r\text{-th random variable} = x, \\
 &\quad (s-r-1) \text{ random variables between } x \text{ and } y, s\text{-th random variable} = y, \\
 &\quad (L-s) \text{ random variables} > y)
 \end{aligned} \tag{32}$$

$$\begin{aligned}
&= \Pr((r-1) \text{ random variables} < x) \Pr(X_{(r)} = x) \\
&\quad \Pr(x < (s-r-1) \text{ random variables} < y) \\
&\quad \Pr(X_{(s)} = y) \Pr((L-s) \text{ random variables} > y). \tag{33}
\end{aligned}$$

Mathematically, the above expression can be formulated as

$$\begin{aligned}
f_{r,s}(x,y) &= \binom{L}{r-1} \binom{L-r+1}{1} \binom{L-r}{s-r-1} \binom{L-s+1}{1} \\
&\quad P^{r-1}(x) p(x) [P(y) - P(x)]^{s-r-1} p(y) (1 - P(y))^{L-s}. \tag{34}
\end{aligned}$$

Now, notice that channels of different users as defined before are ordered random variables. In addition, based on ordered random variables as described above, PDF of new random variables, i.e., w and z , can be obtained as

$$f_r(x) = \binom{M}{r-1} \binom{M-r+1}{1} P^{r-1}(x) p(x) (1 - P(x))^{M-r}, \tag{35}$$

for $r \in \{m, n\}$ and $x \in \{w, z\}$. Furthermore, the joint distribution of w and z is achieved by

$$\begin{aligned}
f_{m,n}(w,z) &= \binom{M}{m-1} \binom{M-m+1}{1} \binom{M-m}{n-m-1} \binom{M-n+1}{1} \\
&\quad P^{m-1}(w) p(w) [P(z) - P(w)]^{n-m-1} p(z) (1 - P(z))^{M-n}. \tag{36}
\end{aligned}$$

Recalling the equation given by (25) and replacing new variables simplifies the sum rate

expression as

$$\begin{aligned}
& \Pr(R_m + R_n < R_m^O + R_n^O) \\
&= \Pr\left(\frac{1+w}{(1+wa_n^2)^2} < \frac{1+z}{(1+za_n^2)^2}\right) \\
&= \Pr\left(a_n^4(z^2 + wz^2 - w^2 - w^2z) + (w-z) - 2a_n^2(w-z) < 0\right) \\
&= \Pr\left(a_n^4(z+w+wz)(z-w) < (z-w)(1-2a_n^2)\right) \\
&= \Pr(z+w+wz < \beta_1), \tag{37}
\end{aligned}$$

where $\beta_1 = \frac{1-2a_n^2}{a_n^4}$. Considering the fact that w and z have met the constraint of $w < z$ and are both positive random variables, results in

$$\begin{aligned}
\Pr(z+w+wz < \beta_1) &= 1 - \Pr(z+w+wz > \beta_1) \\
&= 1 - \left(\int_0^\infty \int_{\frac{\beta_1-z}{1+z}}^z f_{m,n}(w,z) dw dz \right) \\
&= 1 - \left(\int_{\beta_2}^{\beta_1} \int_{\frac{\beta_1-z}{1+z}}^z f_{m,n}(w,z) dw dz + \int_{\beta_2}^\infty \int_{-\infty}^\infty f_{m,n}(w,z) dw dz \right) \\
&= 1 - \left(\int_{\beta_2}^{\beta_1} \int_{\frac{\beta_1-z}{1+z}}^z f_{m,n}(w,z) dw dz + \int_{\beta_2}^\infty f_n(z) dz \right) \tag{38}
\end{aligned}$$

where $f_n(z)$ and $f_{m,n}(w,z)$ can be obtained based on (35) and (36), respectively [46].

In the following, we verify the above derivations with Monte Carlo simulation. Similar to the previous section, we consider ten users and assess the performance of NOMA based on the mentioned probability criteria. In other words, in Fig. 5.7 the power is divided to 1/5 and 4/5.

It can be seen that by reducing the power of noise, i.e., N_0 , the probability that OMA achieves higher sum rate capacity in comparison with NOMA gets smaller. Another observation is that (similar to the previous results) increasing the channel difference experienced by users enhances the performance of NOMA.

Rician channel has been considered in Fig. 5.8 with Rician factor of 5. Comparing Fig. 5.7

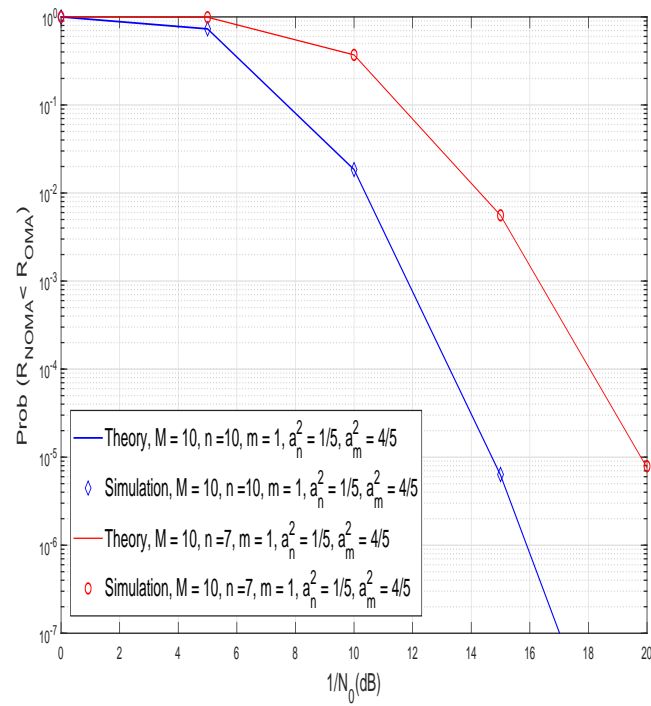


Figure 5.7: Probability of OMA outperforming NOMA vs. $1/N_0$, $K = 0$.

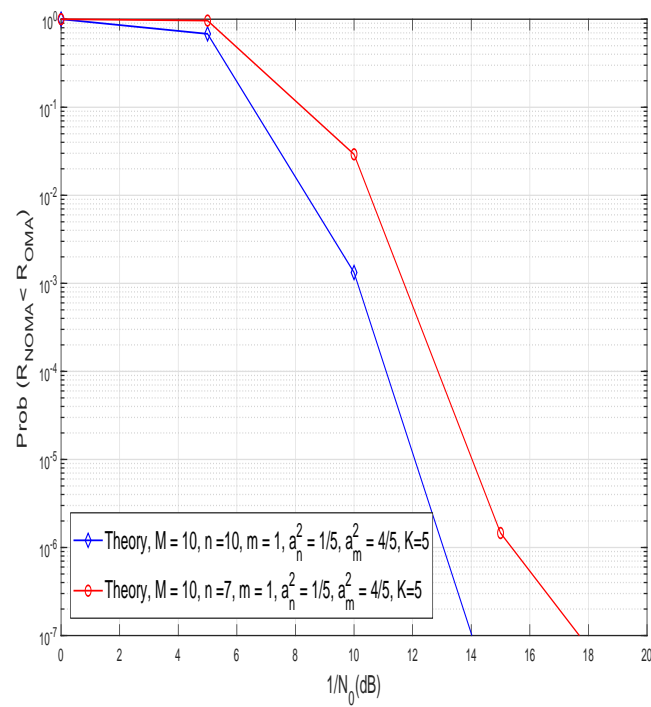


Figure 5.8: Probability of OMA outperforming NOMA vs. $1/N_0$, $K = 5$.

and Fig. 5.8, we can see that although more channel differentiation results in better performance (regardless of Rayleigh and Rician channel), this benefit is more highlighted when the channel realization follows the Rayleigh distribution.

5.4.2 User pairing in MIMO Scenario

In MIMO-NOMA transmission, there are multiple antennas implemented at BS and users. Therefore, the channel between BS and k -th user (for $k \in \{1, \dots, M\}$) is modeled in matrix form, i.e., $\mathbf{H}_1, \dots, \mathbf{H}_M$. One way to order users is based on summation of squared independent sub-channels, which can be calculated in terms of Frobenius norm [48] such that

$$\|\mathbf{H}_1\|_F^2 \leq \dots \leq \|\mathbf{H}_M\|_F^2. \quad (39)$$

In order to implement the above equation, one can consider the variances of elements in channel matrices [49]. In other words, variances need to satisfy the constraint

$$\sigma_1^2 \leq \dots \leq \sigma_M^2, \quad (40)$$

in which σ_k^2 denotes the covariance of the channel between BS and k -th user. Another approach to model the ordered MIMO channel is to consider the path-loss model and thus the users can be ordered in terms of their distances to the BS. For this reason, we consider the following channel model between BS and k -th user:

$$\mathbf{H}_k = \Lambda_k \mathbf{G}_k, \quad (41)$$

where Λ_k denotes the path-loss and we consider it as $\Lambda_k = r_k^{(-\alpha/2)}$, in which r_k is the distance from BS to the k -th user and α is the path-loss exponent.

In the following section, we consider the capacity of SM, which will be used later for the sake of comparison between the performance of NOMA and OMA.

5.5 Capacity of SM-NOMA

Let us start this section by definition and concept of capacity. Practically, capacity is defined as the maximum rate at which information can be transmitted and recovered at the receiver with sufficiently low probability of error [50]. Nevertheless, as explained earlier, the information in SM is conveyed by antenna index as well as constellation space.

In order to calculate the capacity of SM, one approach is to evaluate the probability of error [51, 52] and consider the equation

$$C_{SM} = (m + n) (1 + P_e \log_2(P_e) + P_c \log_2(P_c)), \quad (42)$$

where m and n represent number of input bits conveyed by constellation and antenna space, respectively. In other words, spectral efficiency of the system is $m + n$. P_e denotes the average probability of error (which has been expressed at the beginning of the Chapter) while $P_c = 1 - P_e$ stands for the probability of correct detection.

Alternatively, the formal approach to obtain the capacity of SM is to maximize the mutual information as

$$C_{SM} = \max_{f_S(s), f_L(l)} I(\mathbf{y}; s, l) \quad (43)$$

$$= \max_{f_S(s), f_L(l)} (I(\mathbf{y}; s | l) + I(\mathbf{y}; l)) \quad (44)$$

$$= \max_{f_S(s), f_L(l)} (I_{sym} + I_{ant}), \quad (45)$$

in which the maximization problem is over the PDF of random variables corresponding to the transmitted symbol, $f_S(s)$, and antenna index, $f_L(l)$. In the above equation, I_{sym} represents the mutual information of the received signal and transmitted constellation conditioned on a given antenna index while I_{ant} shows the mutual information of the received signal and antenna index [53].

The first term in (45) can be expressed by

$$I_{sym} = I(\mathbf{y}; s | l) = \sum_{l'=1}^{N_t} p_{l'} I(\mathbf{y}; s | l' = l) \quad (46)$$

$$= \sum_{l'=1}^{N_t} \frac{1}{N_t} \log_2 (1 + \gamma \|\mathbf{h}_{l'}\|^2), \quad (47)$$

where p_l denotes the probability of activating the l -th antenna index. In addition, γ in (47) denotes the SNR/SINR which depends on the order of user in NOMA.

Similar to [53] and for the sake of further illustration, we consider the following sufficient statistical transformation

$$y = \frac{\mathbf{h}_l^H}{\|\mathbf{h}_l\|^2} \mathbf{y}. \quad (48)$$

It is worth mentioning that for a given antenna index, y is a zero-mean complex Gaussian random variable with variance $\sigma_l^2 = 1 + \gamma \|\mathbf{h}_l\|^2$.

The next step is to calculate the second term in (45), i.e., I_{ant} , which is defined by

$$\begin{aligned} I_{ant} = I(\mathbf{y}; l) &= -H(y | l) + H(y) \\ &= \underbrace{-\sum_{l'=1}^{N_t} p_{l'} H(y | l' = l)}_{A_1} - \underbrace{\int f_Y(y) \log_2(f_Y(y)) dy}_{A_2}. \end{aligned} \quad (49)$$

In the above equation A_1 depends on the entropy of a Gaussian distributed random variable y , written as

$$A_1 = \sum_{l'=1}^{N_t} \frac{1}{N_t} \log_2(\pi e \sigma_{l'}^2). \quad (50)$$

Accordingly, we can use the chain rule in the second term of (49) to obtain A_2 as

$$A_2 = \frac{1}{N_t} \sum_{l=1}^{N_t} \int f_{Y|L}(y|l) \log_2 \left(\frac{1}{N_t} \sum_{l'=1}^{N_t} f_{Y|L'}(y|l') \right) dy \quad (51)$$

$$= \frac{1}{N_t} \sum_{l=1}^{N_t} \left(-\log_2(N_t) + \underbrace{E_{Y|L}\{g(y)\}}_{B_2} \right) \quad (52)$$

$$= -\log_2(N_t) + \frac{1}{N_t} \sum_{l=1}^{N_t} \left(\underbrace{E_{Y|L}\{g(y)\}}_{B_2} \right), \quad (53)$$

where

$$g(y) = \log_2 \left(\sum_{l'=1}^{N_t} \frac{1}{\pi \sigma_{l'}^2} e^{-\frac{|y|^2}{\sigma_{l'}^2}} \right). \quad (54)$$

Notice that y as defined in (48) is a complex random variable with real and imaginary components shown by y_1 and y_2 , respectively. As given in [53], we consider the Taylor series expansion of $g(y)$ over the mean of random variable y , i.e., 0, followed by the expectation to calculate B_2 as expressed in (53) by

$$B_2 = E_Y \{T(g, y, 0)\} = \sum_{n=0}^{\infty} \frac{1}{n!} \sum_{m=1}^2 \frac{\partial^n g}{\partial y_m^n}(0) E\{(y_m - 0)^n\}. \quad (55)$$

In the above equation, $T\{\cdot\}$ stands for the Taylor series expansion. Notice that, since y is zero-mean random variable, $E\{(y_m - 0)^n\}$ denotes the n -th central moment of y_m [54], and can be mathematically written as

$$E\{(y_m - 0)^n\} = \vartheta_{y_m}^n = \begin{cases} (n-1)!! \frac{\sigma_l^n}{2^{\frac{n}{2}}} & \text{for } n \text{ is even} \\ 0 & \text{for } n \text{ is odd} \end{cases} \quad (56)$$

for $m \in \{1, 2\}$. In (56), $(\cdot)!!$ stands for double factorial. Considering the following equality

$$(2n-1)!! = \frac{(2n)!}{2^n n!}, \quad (57)$$

defining new variable as $n = 2k$, and assuming symmetric derivative, i.e., $\frac{\partial^n g}{\partial y_1^n} = \frac{\partial^n g}{\partial y_2^n}$, the expect-

tation in (55) is

$$E_Y \{T(g, y, 0)\} = \sum_{k=0}^{\infty} \frac{\partial^{2k} g}{\partial y_1^{2k}}(0) \frac{\sigma_l^{2k} (2k-1)!!}{2^{k-1} (2k)!} \quad (58)$$

$$= \sum_{k=0}^{\infty} \frac{\partial^{2k} g}{\partial y_1^{2k}}(0) \frac{\sigma_l^{2k}}{2^{k-1} 2^k k!} \quad (59)$$

$$= \sum_{k=0}^{\infty} \frac{\partial^{2k} g}{\partial y_1^{2k}}(0) \frac{\sigma_l^{2k}}{2^{2k-1} k!} \quad (60)$$

$$= \log_2 \left(\sum_{l'=1}^{N_t} \frac{1}{\pi \sigma_{l'}^2} \right) + \sum_{k=1}^{\infty} \frac{\partial^{2k} g}{\partial y_1^{2k}}(0) \frac{\sigma_l^{2k}}{2^{2k-1} k!}$$

where equation (59) is achieved by replacing (57) in (58). Moreover, the first term in (60) is derived by setting $y = 0$ in (54).

Having above equations, the mutual information between y and antenna index can be written as given in [53] by

$$I_{ant} = - \sum_{l'=1}^{N_t} \frac{1}{N_t} \log_2(\pi e \sigma_{l'}^2) + \log_2(N_t) - \log_2 \left(\sum_{l'=1}^{N_t} \frac{1}{\pi \sigma_{l'}^2} \right) - \frac{1}{N_t} \sum_{l=1}^{N_t} \left(\sum_{k=1}^{\infty} \frac{\partial^{2k} g}{\partial y_1^{2k}}(0) \frac{\sigma_l^{2k}}{2^{2k-1} k!} \right). \quad (61)$$

Finally, replacing (61) and (47) in (45), and considering the second order approximation results in the following capacity expression [53]

$$C_{SM} \simeq \log_2(H(\boldsymbol{\sigma}^2)) - \frac{1}{\log 2} \left(1 - A(\boldsymbol{\sigma}^2) \frac{H(\boldsymbol{\sigma}^2)}{H(\boldsymbol{\sigma}^4)} \right) \quad (62)$$

in which $\boldsymbol{\sigma}_n = (\sigma_1^n, \dots, \sigma_{N_t}^n)^T$. Notice that in above equation, $A(\cdot)$ and $H(\cdot)$ represent the arithmetic and harmonic mean expressions, respectively.

5.5.1 Simulation Results

In this section, we evaluate the effect of user pairing based on the derived capacity equations in the last section. In particular, we calculate the sum rate capacity of two users with different channel strengths and make the observation that which two pairs of users results in higher achievable rate. To this end, we consider the path-loss model as defined in (41). In addition, we assume the second user with poor channel experience is located in a fixed place i.e., in distance of 100 meter, while the distance of the user with strong channel varies, i.e., from 30m to 90m. We assume the path-loss exponent of 3.6. We also assume that the power has been divided to $1/5$ and $4/5$, based on which we plot the sum capacity of different sets of users in Fig. 5.9. It has been shown that as the distance between two users increases (which means their experienced channel is more different), the overall capacity increases. This results is identical to the conventional NOMA system with antenna selection and multiplexing.

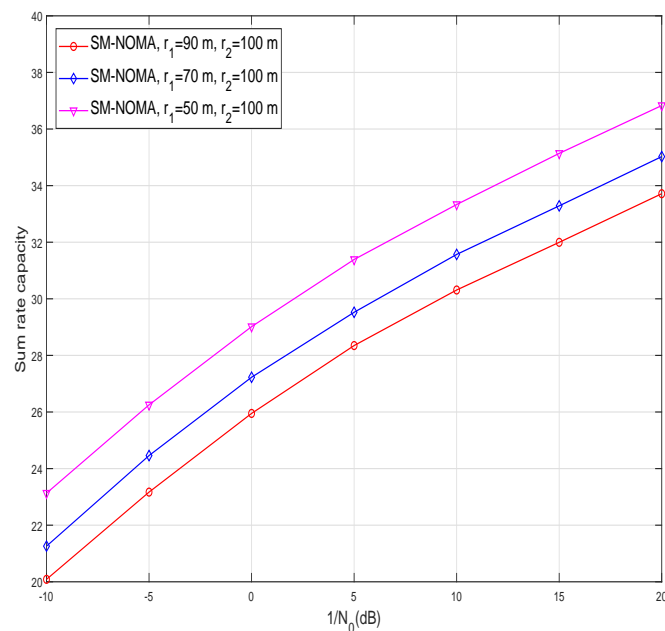


Figure 5.9: User pairing based on sum rate capacity, $\alpha_1^2 = 1/5$ and $\alpha_2^2 = 4/5$, $N_t = Nr = 4$.

In Fig. 5.10, we made the comparison on performance of SM-NOMA and SM-OMA. Similar to Fig. 5.9, we consider fixed and variable distances for the second user and first user,

respectively. One can see from this Figure that for all scenarios, SM-NOMA outperform SM-OMA.

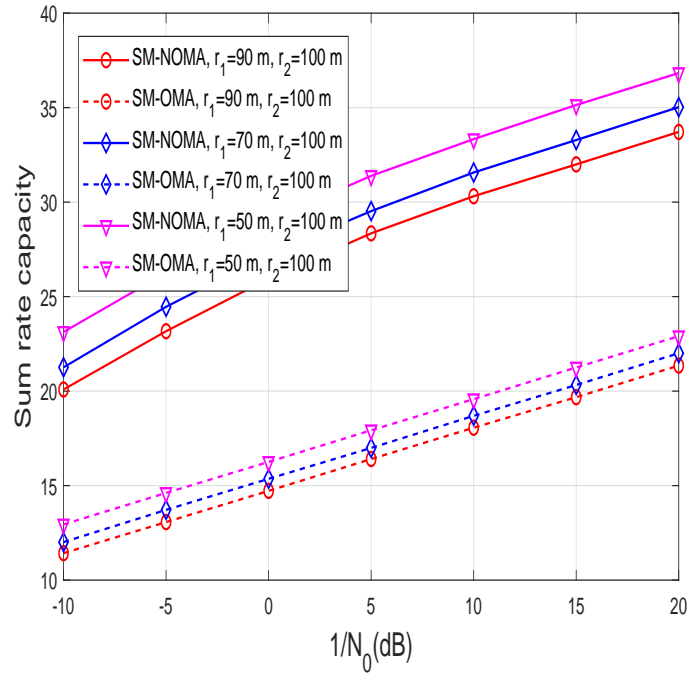


Figure 5.10: Capacity comparison between SM-NOMA and SM-OMA, $\alpha_1^2 = 1/5$ and $\alpha_2^2 = 4/5$, $N_t = N_r = 4$.

Chapter 6

Conclusion and Future Work

In this thesis, we investigate on the challenges of future advanced communication systems, namely limited available power (which create the limitation in number of RF chains) and spectrum scarcity. In order to overcome these problems, we propose different approaches in Chapters 3-5.

In Chapter 3, we propose the antenna grouping for MIMO systems with dual-polarized antenna elements combined with GSM transmission scheme. In particular, polarization, which is an inherent component of a waveform, has been exploited as an additional degree of freedom while dual-polarized antennas occupies less space in comparison with uni-polarized antenna with same virtual number of antenna elements. Furthermore, applying GSM enables us to reduce the number of RF chains which results in energy and power efficiency. Considering the fact that not all antenna subsets in GSM have the optimal performance, we use the circle packing method to group the DP antennas in such a way that the optimum performance is achieved in GSM transmission.

In Chapter 4, a novel beamforming-based network coexistence has been proposed to alleviate the interference which is generated as a results of spectrum scarcity and LTE spectrum shift from licensed to unlicensed band. We have approached to this problem and found the beamforming vectors from two different points of view. In the first procedure, we have optimized the coefficients such that the disruptive LTE power received by the Wi-Fi AP is minimized. In the second method, the beamformer is designed to maximize the received SNR at LTE user's. Both approaches enable Wi-Fi AP to sense the channel as if it is empty and eliminate the protocol

modification which results in a cost-efficient coexistence.

The last contribution of this thesis is to tackle the spectrum scarcity based on overlapped resource allocation to users with different channel qualities. More specifically, we have focused on users with limited number of RF chains. Thus, in order to preserve the limited RF chains while maintaining the spectral efficiency, we apply SM-based transmission under NOMA scheme and evaluate the performance of users followed by capacity analysis to elaborate the impact of user pairing.

While our proposed solutions touch some of the main challenges in next generation of wireless communication, there is potential for further investigations. In particular, in Chapter 3, we have consider the given number of available RF chains. Nevertheless, more study can be conducted to investigate the trade off between number of activated antennas within each antenna group and the performance.

Chapter 4 can be more extended for the case where LTE BS contains massive number of antennas and hybrid beamforming or GSM can be implemented to satisfy the practical implementation constraints related to limited number of RF chains. In addition, other criteria such as Wi-Fi throughput or the probability of collision can be investigated. There is also potential for in depth investigation on the interference from other users with channel model including path-loss.

The SM-based NOMA approach as described in Chapter 5 can be further investigated from power allocation point of view. In particular, the strategy in which the total power can be split between two user can be studied such that it maximizes the overall sum rate capacity.

Bibliography

- [1] M. Di Renzo, H. Haas, A. Ghrayeb, S. Sugiura, and L. Hanzo, “Spatial modulation for generalized mimo: Challenges, opportunities, and implementation,” *Proceedings of the IEEE*, vol. 102, no. 1, pp. 56–103, 2014.
- [2] Y. S. Cho, J. Kim, W. Y. Yang, and C. G. Kang, *MIMO-OFDM Wireless Communications with MATLAB*. Wiley Publishing, 2010.
- [3] E. Basar, M. Wen, R. Mesleh, M. D. Renzo, Y. Xiao, and H. Haas, “Index modulation techniques for next-generation wireless networks,” *IEEE Access*, vol. 5, pp. 16 693–16 746, 2017.
- [4] A. A. Giordano and A. H. Levesque, *Modeling of Digital Communication Systems Using SIMULINK*, ser. Digital communications – Computer simulation. Wiley, 2015, no. v. 1. [Online]. Available: <http://ebookcentral.proquest.com/lib/west/detail.action?docID=1895906>
- [5] Y. Saito, Y. Kishiyama, A. Benjebbour, T. Nakamura, A. Li, and K. Higuchi, “Non-orthogonal multiple access (noma) for cellular future radio access,” in *2013 IEEE 77th Vehicular Technology Conference (VTC Spring)*, June 2013, pp. 1–5.
- [6] Statista. (2018) Dc. global telecom services spending forecast from 2014 to 2020 (in billion u.s. dollars). [Online]. Available: <https://www.statista.com/statistics/322995/worldwide-telecom-services-spending-forecas>

- [7] J. G. Andrews, S. Buzzi, W. Choi, S. V. Hanly, A. Lozano, A. C. K. Soong, and J. C. Zhang, "What will 5g be?" *IEEE Journal on Selected Areas in Communications*, vol. 32, no. 6, pp. 1065–1082, June 2014.
- [8] M. M. A. Hossain and R. Jntti, "Impact of efficient power amplifiers in wireless access," in *2011 IEEE Online Conference on Green Communications*, Sept 2011, pp. 36–40.
- [9] C. Sexton, N. J. Kaminski, J. M. Marquez-Barja, N. Marchetti, and L. A. DaSilva, "5g: Adaptable networks enabled by versatile radio access technologies," *IEEE Communications Surveys Tutorials*, vol. 19, no. 2, pp. 688–720, Secondquarter 2017.
- [10] J. Jeganathan, A. Ghrayeb, L. Szczecinski, and A. Ceron, "Space shift keying modulation for mimo channels," *IEEE Transactions on Wireless Communications*, vol. 8, no. 7, pp. 3692–3703, July 2009.
- [11] J. Jeganathan, A. Ghrayeb, and L. Szczecinski, "Generalized space shift keying modulation for mimo channels," in *2008 IEEE 19th International Symposium on Personal, Indoor and Mobile Radio Communications*, Sept 2008, pp. 1–5.
- [12] R. Mesleh, H. Haas, S. Sinanovic, C. W. Ahn, and S. Yun, "Spatial modulation," *IEEE Trans. on Vehicular Tech.*, vol. 57, no. 4, pp. 2228–2241, July 2008.
- [13] M. Koca and H. Sari, "Generalized spatial modulation over correlated fading channels: Performance analysis and optimization," in *Telecommunications (ICT), 2013 20th International Conference on*, May 2013, pp. 1–5.
- [14] J. Jeganathan, A. Ghrayeb, and L. Szczecinski, "Spatial modulation: optimal detection and performance analysis," *IEEE Communications Letters*, vol. 12, no. 8, pp. 545–547, Aug 2008.
- [15] R. Mesleh, H. Haas, C. W. Ahn, and S. Yun, "Spatial modulation - a new low complexity spectral efficiency enhancing technique," in *2006 First International Conference on Communications and Networking in China*, Oct 2006, pp. 1–5.

- [16] D. A. Basnayaka and H. Haas, "Spatial modulation for massive mimo," in *2015 IEEE International Conference on Communications (ICC)*, June 2015, pp. 1945–1950.
- [17] R. Rajashekar, K. V. S. Hari, and L. Hanzo, "Antenna selection in spatial modulation systems," *IEEE Communications Letters*, vol. 17, no. 3, pp. 521–524, March 2013.
- [18] X. Wu, M. D. Renzo, and H. Haas, "Adaptive selection of antennas for optimum transmission in spatial modulation," *IEEE Transactions on Wireless Communications*, vol. 14, no. 7, pp. 3630–3641, July 2015.
- [19] T. Handte, A. Muller, and J. Speidel, "Ber analysis and optimization of generalized spatial modulation in correlated fading channels," in *Vehicular Technology Conference Fall (VTC 2009-Fall), 2009 IEEE 70th*, Sept 2009, pp. 1–5.
- [20] A. Younis, N. Serafimovski, R. Mesleh, and H. Haas, "Generalised spatial modulation," in *2010 Conference Record of the Forty Fourth Asilomar Conference on Signals, Systems and Computers*, Nov 2010, pp. 1498–1502.
- [21] A. Younis, R. Mesleh, M. D. Renzo, and H. Haas, "Generalised spatial modulation for large-scale mimo," in *2014 22nd European Signal Processing Conference (EUSIPCO)*, Sept 2014, pp. 346–350.
- [22] J. Park and B. Clerckx, "Multi-user linear precoding for multi-polarized massive mimo system under imperfect csit," *IEEE Transactions on Wireless Communications*, vol. 14, no. 5, pp. 2532–2547, May 2015.
- [23] C. Oestges, B. Clerckx, M. Guillaud, and M. Debbah, "Dual-polarized wireless commun.: from propagation models to system performance evaluation," *IEEE Trans. on Wireless Commun.*, vol. 7, no. 10, pp. 4019–4031, Oct. 2008.
- [24] M. Coldrey, "Modeling and capacity of polarized mimo channels," in *IEEE Vehicular Tech. Conf. (VTC)-Spring*, May 2008, pp. 440–444.
- [25] G. Zafari, M. Koca, and H. Sari, "Spatial modulation with dual-polarized antennas," in *2015 IEEE International Conference on Communications (ICC)*, June 2015, pp. 2375–2380.

- [26] ———, “Dual-polarized spatial modulation over correlated fading channels,” *IEEE Transactions on Communications*, vol. 65, no. 3, pp. 1336–1352, March 2017.
- [27] A. Habib, “Multiple polarized mimo with antenna selection,” in *2011 18th IEEE Symposium on Communications and Vehicular Technology in the Benelux (SCVT)*, Nov 2011, pp. 1–8.
- [28] H. Asplund, J. E. Berg, F. Harrysson, J. Medbo, and M. Riback, “Propagation characteristics of polarized radio waves in cellular communications,” in *IEEE 66th Vehicular Technology Conference, VTC 2007*, Sept 2007, pp. 839–843.
- [29] G. Proakis, *Digital Commun.*, 4th ed. McGraw- Hill Higher Education, 2000.
- [30] M. Koca and H. Sari, “Performance of spatial modulation over correlated fading channels with channel estimation errors,” in *2013 IEEE Wireless Communications and Networking Conference (WCNC)*, April 2013, pp. 3937–3942.
- [31] T. J. Barnett, A. Sumits, S. Jain, and U. Andra, “Cisco Visual Networking Index (VNI) Update Global Mobile Data Traffic Forecast,” *Vni*, pp. 2015–2020, 2015. [Online]. Available: <http://www.cisco.com/c/en/us/solutions/collateral/service-provider/visual-networking-index-vni/complete-white-paper-c11-481360.html>
- [32] Q. Incorporated, “Extending LTE Advanced to unlicensed spectrum December 2013,” no. December, pp. 1–12, 2013.
- [33] J. Li, X. Wang, D. Feng, M. Sheng, and T. Q. S. Quek, “Share in the commons: Coexistence between lte unlicensed and wi-fi,” *IEEE Wireless Communications*, vol. 23, no. 6, pp. 16–23, December 2016.
- [34] A. M. Cavalcante, E. Almeida, R. D. Vieira, F. Chaves, R. C. D. Paiva, F. Abinader, S. Choudhury, E. Tuomaala, and K. Doppler, “Performance evaluation of LTE and Wi-Fi coexistence in unlicensed bands,” *IEEE Vehicular Technology Conference*, no. November 2014, pp. 54–61, 2013.

- [35] J. Jeon, Q. C. Li, H. Niu, A. Papathanassiou, and G. Wu, "LTE in the unlicensed spectrum: A novel coexistence analysis with WLAN systems," *2014 IEEE Global Communications Conference, GLOBECOM 2014*, pp. 3459–3464, 2014.
- [36] L. Li, A. H. Jafari, X. Chu, and J. Zhang, "Simultaneous transmission opportunities for LTE-LAA smallcells coexisting with WiFi in unlicensed spectrum," *2016 IEEE International Conference on Communications, ICC 2016*, 2016.
- [37] Takehiro Nakamura, "Proposal for Candidate Radio Interface Technologies for IMT-Advanced Based on LTE Release 10 and Beyond Takehiro Nakamura," *ITU-R WP 5D 3rd Workshop on IMT-Advanced*, no. ., pp. 17–18, 2009. [Online]. Available: http://3gppmob.etsiqa.org/IMG/pdf/2009_10_3gpp_IMT.pdf
- [38] T. W. Paper, "802.11ac: The Fifth Generation of Wi-Fi," no. March, pp. 1–25, 2014. [Online]. Available: http://www.cisco.com/c/en/us/products/collateral/wireless/aironet-3600-series/white_paper_c11-713103.pdf
- [39] V. Havary-Nassab, S. Shahbazpanahi, A. Grami, and Z. Q. Luo, "Distributed beamforming for relay networks based on second-order statistics of the channel state information," *IEEE Transactions on Signal Processing*, vol. 56, no. 9, pp. 4306–4316, 2008.
- [40] J. Ryu, C. Joo, T. T. Kwon, N. B. Shroff, and Y. Choi, "Distributed sinr based scheduling algorithm for multi-hop wireless networks," in *Proceedings of the 13th ACM International Conference on Modeling, Analysis, and Simulation of Wireless and Mobile Systems*, ser. MSWIM '10. New York, NY, USA: ACM, 2010, pp. 376–380. [Online]. Available: <http://doi.acm.org/10.1145/1868521.1868583>
- [41] S. Timotheou and I. Krikidis, "Fairness for non-orthogonal multiple access in 5g systems," *IEEE Signal Processing Letters*, vol. 22, no. 10, pp. 1647–1651, Oct 2015.
- [42] S. Chen, B. Ren, Q. Gao, S. Kang, S. Sun, and K. Niu, "Pattern division multiple access - a novel nonorthogonal multiple access for fifth-generation radio networks," *IEEE Transactions on Vehicular Technology*, vol. 66, no. 4, pp. 3185–3196, April 2017.

- [43] Z. Ding, M. Peng, and H. V. Poor, "Cooperative non-orthogonal multiple access in 5g systems," *IEEE Communications Letters*, vol. 19, no. 8, pp. 1462–1465, Aug 2015.
- [44] I. M. Jacobs and J. M. Wozencraft, *Principles of communication engineering*. New York, NY: Wiley, 1965. [Online]. Available: <https://cds.cern.ch/record/105069>
- [45] V. V. Veeravalli, "On performance analysis for signaling on correlated fading channels," *IEEE Transactions on Communications*, vol. 49, no. 11, pp. 1879–1883, Nov 2001.
- [46] Z. Ding, P. Fan, and H. V. Poor, "Impact of user pairing on 5g nonorthogonal multiple-access downlink transmissions," *IEEE Transactions on Vehicular Technology*, vol. 65, no. 8, pp. 6010–6023, Aug 2016.
- [47] H. David and H. Nagaraja, *Order Statistics*, ser. Wiley Series in Probability and Statistics. Wiley, 2004. [Online]. Available: <https://books.google.ca/books?id=bdhzFXg6xFkC>
- [48] C. L. Wang, J. Y. Chen, and Y. J. Chen, "Power allocation for a downlink non-orthogonal multiple access system," *IEEE Wireless Communications Letters*, vol. 5, no. 5, pp. 532–535, Oct 2016.
- [49] Q. Sun, S. Han, C. L. I, and Z. Pan, "On the ergodic capacity of mimo noma systems," *IEEE Wireless Communications Letters*, vol. 4, no. 4, pp. 405–408, Aug 2015.
- [50] T. M. Cover and J. A. Thomas, *Elements of Information Theory*, ser. Digital communications – Computer simulation. John Wiley & Sons, Inc., 2005, no. v. 2. [Online]. Available: <http://dx.doi.org/10.1002/047174882X.biblio>
- [51] E. Soujeri and G. Kaddoum, "The impact of antenna switching time on spatial modulation," *IEEE Wireless Communications Letters*, vol. 5, no. 3, pp. 256–259, June 2016.
- [52] F. A. Prisecaru, "Mutual information and capacity of spatial modulation systems."
- [53] P. Henarejos and A. I. Prez-Neira, "Capacity analysis of index modulations over spatial, polarization, and frequency dimensions," *IEEE Transactions on Communications*, vol. 65, no. 12, pp. 5280–5292, Dec 2017.

- [54] J. A. Gubner, *Probability and Random Processes for Electrical and Computer Engineers*.
New York, NY, USA: Cambridge University Press, 2006.

Curriculum Vitae

Name: Golara Zafari

Post-Secondary Education and Degrees: The University of Western Ontario
London, Ontario, Canada
May. 2016 - date MSc.

Boğaziçi University
Istanbul, Turkey
2012 - 2014 MSc.

Khaje Nasir Tousi University of Technology
Tehran, Iran
2007 - 2011 BSc.

Honours and Awards: WGRS
2016-2018

Related Work Experience: Teaching Assistant
The University of Western Ontario
2016 - 2018

Research Assistant
The University of Western Ontario

2016 - 2018

Research Assistant

Boğaziçi University

2012 - 2016

Publications:

- [1] G. Zafari, M. Koca and H. Sari, "Spatial modulation with dual-polarized antennas," 2015 IEEE International Conference on Communications (ICC), London, 015, pp. 2375-2380.
- [2] G. Zafari, M. Koca and H. Sari, "Dual-Polarized Spatial Modulation Over Correlated Fading Channels," in IEEE Transactions on Communications, vol. 65, no. 3, pp. 1336-1352, March 2017.
- [3] G. Zafari, M. Koca, X. Wang and M. G. S. Sriyananda, "Antenna Grouping in Dual-Polarized Generalized Spatial Modulation," 2017 IEEE 86th Vehicular Technology Conference (VTC-Fall), Toronto, ON, 2017, pp. 1-6.
- [4] G. Zafari and X. Wang, "Cognitive Co-Existence of Unlicensed Wireless Networks through Beamforming," 2017 IEEE 86th Vehicular Technology Conference (VTC-Fall), Toronto, ON, 2017, pp. 1-5.